UPPSALA
UNIVERSITET

Digital Comprehensive Summaries of Uppsala Dissertations from the Faculty of Science and Technology 732

Ultrasonic Arrays for Sensing and Beamforming of Lamb Waves

MARCUS ENGHOLM

ACTA
UNIVERSITATIS
UPSALIENSIS
UPPSALA
2010

ISSN 1651-6214
ISBN 978-91-554-7785-1
urn:nbn:se:uu:diva-122189

Dissertation presented at Uppsala University to be publicly examined in Siegbahnsalen, Lägerhyddsvägen 1, Uppsala, Friday, May 21, 2010 at 13:15 for the degree of Doctor of Philosophy. The examination will be conducted in English.

Abstract
Engholm, M. 2010. Ultrasonic Arrays for Sensing and Beamforming of Lamb Waves. Acta Universitatis Upsaliensis. *Digital Comprehensive Summaries of Uppsala Dissertations from the Faculty of Science and Technology* 732. 83 pp. Uppsala. ISBN 978-91-554-7785-1.

Non-destructive testing (NDT) techniques are critical to ensure integrity and safety of engineered structures. Structural health monitoring (SHM) is considered as the next step in the field enabling continuous monitoring of structures.

The first part of the thesis concerns NDT and SHM using guided waves in plates, or Lamb waves, to perform imaging of plate structures. The imaging is performed using a fixed active array setup covering a larger area of a plate. Current methods are based on conventional beamforming techniques that do not efficiently exploit the available data from the small arrays used for the purpose. In this thesis an adaptive signal processing approach based on the minimum variance distortionless response (MVDR) method is proposed to mitigate issues related to guided waves, such as dispersion and the presence of multiple propagating modes. Other benefits of the method include a significant increase in resolution. Simulation and experimental results show that the method outperforms current standard processing techniques.

The second part of the thesis addresses transducer design issues for resonant ultrasound inspections. Resonant ultrasound methods utilize the shape and frequency of the object's natural modes of vibration to detect anomalies. The method considered in the thesis uses transducers that are acoustically coupled to the inspected structures. Changes in the transducer's electrical impedance are used to detect defects. The sensitivity that can be expected from such a setup is shown to highly depend on the transducer resonance frequency, as well as the working frequency of the instrument. Through simulations and a theoretical argumentation, optimal conditions to achieve high sensitivity are given.

Keywords: imaging, array processing, guided waves, Lamb waves, dispersive waves, multi-modal waves, spatial filtering, mode suppression, resonant ultrasound, transducer design, direction of arrival estimation, adaptive beamforming

Marcus Engholm, Signals and Systems Group, Box 528, Uppsala University, SE-75120 Uppsala, Sweden

ISSN 1651-6214
ISBN 978-91-554-7785-1
urn:nbn:se:uu:diva-122189 (http://urn.kb.se/resolve?urn=urn:nbn:se:uu:diva-122189)

to Annelie, Elias & Filip

List of Papers

This thesis is based on the following papers, which are referred to in the text by their Roman numerals.

I **Engholm, M.**, Stepinski, T. (2010) Direction of Arrival Estimation of Lamb Waves Using Circular Arrays. Recommended for publication in *Structrual Health Monitoring*.

II **Engholm, M.**, Stepinski, T. (2010) Adaptive Beamforming for Array Imaging of Plate Structures Using Lamb Waves. Recommended for publication in *IEEE Transactions on Ultrasonics, Ferroelectrics, and Frequency Control*.

III **Engholm, M.**, Stepinski, T., Olofsson, T. (2010) Imaging and Suppression of Lamb Modes Using Multiple Transmitter Adaptive Beamforming. In manuscript.

IV Stepinski, T., **Jonsson, M.** (2005) Narrowband ultrasonic spectroscopy for NDE of layered structures. *INSIGHT, the Journal of The British Institute of Non-Destructive Testing*, 47(4):220–225.

V **Engholm, M**., Stepinski, T. (2005) Designing and evaluating transducers for narrowband ultrasonic spectroscopy. *2005 IEEE Ultrasonics Symposium*, 4:2085 - 2088 .

VI **Engholm, M.**, Stepinski, T. (2007) Designing and evaluating transducers for narrowband ultrasonic spectroscopy. *NDT & E International*, 40(1):49–56.

Contents

1. Introduction

Plate structures are everywhere in the world around us. Cars, ships, airplanes, and pressure vessels are only a few examples of vehicles and engineered structures consisting of a considerable amount of flat or slightly curved plates. These are often required to have a significant life span. For instance, it is not uncommon for airplanes to be in service for over 20 years. During that time, the high safety standards required by governments and consumers need to be complied, requiring frequent maintenance and inspection of critical areas. This, among many other applications, has triggered the development of testing methods that can assess the state of a structure or material without affecting its functionality, so called non-destructive testing (NDT).

1.1 Non-destructive testing

During the last century, a large number of NDT techniques were developed. One technique that has proven to be very versatile for many different applications is the use of high frequency, or *ultrasonic*, elastic waves. Ultrasonic inspection is commonly performed by transmitting an ultrasonic pulse into the inspected object, which is reflected, or *backscattered*, at discontinuities within object. These echoes are received and analysed in time to search for echoes that can indicate the presence of defects.

The generation and detection of ultrasonic waves is performed using transducers that provide the means for converting electric signals into elastic waves and vice versa. This transduction can be accomplished using a number of different physical principles. For example, piezoelectric transducers convert electrical energy to mechanical energy in a piezoelectric element, in contrast to electromechanical acoustic transducers (EMAT) that generate and detect elastic waves in a metallic object through magnetic fields, making the actual transduction occur inside the object.

Ultrasonic inspections can be performed in a number of different configurations, such as, pulse-echo or pitch-catch, as illustrated in Figure 1.1. A pulse-echo setup uses a single transducer that both transmits and receives the pulse. Pitch-catch setups, on the other hand, use a separate receiving transducer.

Inspections require much manual labour and during that time the inspected object may be inoperable. In the last two decades, a considerable amount of research has been conducted on techniques for the use of permanently attached

devices capable of continuous monitoring of structures, so called structural health monitoring (SHM). The benefits of such an approach are improved safety and reduced costs by early warning of potential problems [1]. This could also reduce the frequency of manual inspections that can be extremely time consuming if large areas require inspection. The work presented in this thesis is highly relevant for, but not limited to, SHM.

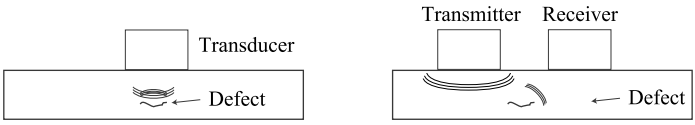

Figure 1.1: Pulse based inspections. Pulse-echo setup (left) and pitch-catch setup (right).

1.2 Lamb wave imaging

Several of the available NDT methods, such as eddy current testing, can only detect defects directly under the probe. Although precise localization and, in many cases, high sensitivity can be achieved, it makes inspection of large plate structures extremely time consuming. An alternative to these types of methods is using ultrasonic guided waves. Guided waves can potentially propagate over long distances and can therefore be used for rapid inspection of large areas of an object. Examples of applications which benefit from guided waves include long range testing of pipes and rails [2]. A literature survey and summary of guided wave applications can be found in [3].

Guided waves in plate structures, so called *Lamb waves*, have been of considerable interest for NDT during the last few decades. Probably the earliest experimental work on ultrasonic Lamb waves was done by Worlton who proposed their application for NDT in 1961 [4]. In the same manner as for bulk waves illustrated above, Lamb wave inspections can be performed in either pulse-echo, as illustrated in Figure 1.2, or pitch-catch configuration.

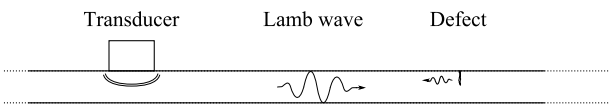

Figure 1.2: Principle of pulse-echo Lamb wave inspection. The guided wave propagates in the plate and is reflected at discontinuities.

Applications employing Lamb waves for NDT include testing and evaluation of adhesive bonds [5, 6, 7], isotropic plates [8, 9, 10], and compos-

ites [11, 12, 13]. Furthermore, Lamb waves ability to propagate over long distances, and thereby enabling wide area coverage, has resulted in a significant amount of research on their application in SHM. A review of work concerning Lamb wave structural health monitoring can be found in [14].

The first part of this thesis concerns a particular application of Lamb waves: imaging. Imaging in general is the representation of an object's externals or internals in the form of an image. Through the ability of Lamb wave to propagate over large distances, an array of transducers capable of transmitting and receiving Lamb waves in arbitrary directions, enables acquisition of backscattered data from a large area around the array. An illustration of such a setup is shown in Figure 1.3. The backscattered waves will consist of reflections from boundaries, such as edges, welds, or defects. Processing of such data enables estimation of amplitudes and positions of scatterers in the region of interest (ROI). However, Lamb wave propagation and interaction with discontinuities is very complex, which complicates acquisition and the following reconstruction of an accurate image.

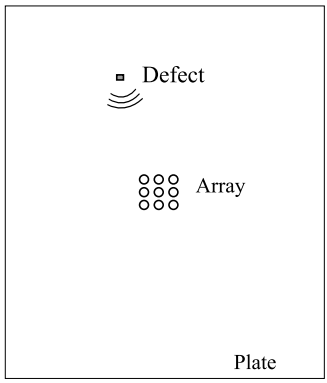

Figure 1.3: One or multiple elements in an array generate Lamb waves that propagate in the plate. The array elements receive the backscattered signals enabling estimation of the position and size of a potential defect.

In traditional applications using arrays, as for instance in radar and sonar, as well as in ultrasonic testing in bulk materials, one dimensional (1D) arrays are commonly used. Such arrays consist of elements along a line. Arrays used for the type of inspection, or monitoring, considered in this thesis should preferably allow omni-directional coverage. As will be discussed in Chapter 3, omni-directional coverage requires the use of two dimensional (2D) arrays, that is, arrays that have its elements distributed in two dimensions, for example circular arrays. However, a significant number of elements in the 2D array is required to achieve sufficient resolution. Previous work on imaging of Lamb waves has mainly been focused on basic array processing methods that may not fully exploit the potential of the setup. In this thesis, more advanced meth-

ods are considered that better utilize the available data to improve resolution and reduce noise in the resulting image.

1.3 Resonance testing

The first section described the use of ultrasonic pulses to interrogate the inside of an object in the search of defects. An alternative to the pulse-based, time domain, techniques are methods concerning the extraction of information contained in an object's natural modes of vibration. The resonance frequencies are directly related to the structure's material properties, such as thickness and elasticity. Defects in a structure will affect its vibrational modes which can be used to assess its condition.

The most common application for this type of methods is the inspection of bonded joints and composites. Defects, such as disbonds or voids in adhesive layers, are in many cases readily detected with these techniques since such defects cause a significant change in the structure's vibrational modes. The basic principle of resonance tests is to measure the electrical impedance response of a transducer that is acoustically coupled to the structure as illustrated in Figure 1.4. Acoustic coupling is achieved through a thin layer of couplant, for example water. Resonances occur at frequencies where the transducer's impedance reaches minima. Changes in the structure directly under the transducer will affect the electrical impedance of the transducer, which can be used to detect defects. Compared to Lamb waves that propagate in the plate, this type of inspections are local.

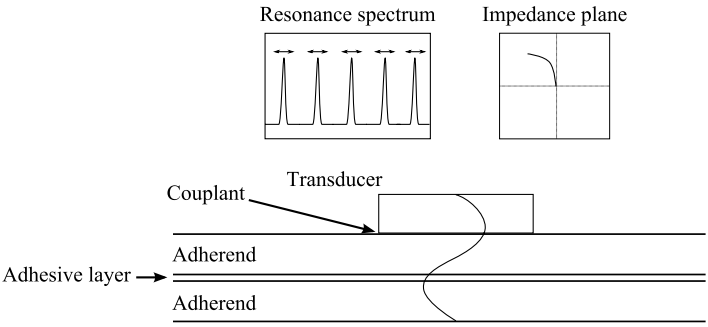

Figure 1.4: A transducer is coupled to the inspected structure by a thin layer of, e.g. water. The transducer is excited by a frequency sweep or a fixed frequency. Changes in resonance frequency or complex transducer impedance are used to detect defects.

This principle can be used in two ways. Instruments, such as, the Fokker bond tester, tracks the transducer's resonance frequency for changes that indicates anomalies in the structure. Other instruments, for example the

BondaScope 3100[1], tracks the complex electrical impedance at a single frequency and displays it in the complex impedance plane.

The second part of this thesis concerns the evaluation of the complex impedance approach. Considerations concerning frequency selection and properties of the transducers to maximize the sensitivity of the measurement are presented.

[1]NDT Systems, Inc.

1.4 Comments on the author's contributions

The author's contributions to the respective papers are summarized below.

I	Ideas (except phase-mode approach), experimental setup design and construction, software implementation, simulations, measurements, interpretation, major part of writing
II	Ideas, experimental setup design and construction, software implementation, simulations, measurements, interpretation, major part of writing
III	Ideas, experimental setup design and construction, software implementation, simulations, interpretation, major part of writing
IV	Measurements, parts of software implementation, simulations
V	Idea, software implementation, simulations, interpretation, major part of writing
VI	Idea, software implementation, simulations, interpretation, major part of writing

1.5 Thesis outline

Since most readers interested in this thesis are probably familiar with *either* Lamb waves *or* beamforming methods, but not both, the first two chapters provide a basic introduction into the subjects.

This thesis is organized as follows:

- Chapter 2 gives an overview of important properties of Lamb waves relevant for the work.
- Chapter 3 introduces the basic concept of both conventional beamforming and adaptive methods. It also serves as a preparation for Chapter 5 by bringing to attention some issues that need to be addressed when employing these techniques for active array imaging.
- Chapter 4 provides a short overview of important previous work on Lamb wave imaging with emphasis on arrays.
- Chapter 5 explains the issues related to Lamb waves that need to be considered when using adaptive methods on Lamb waves and the steps that resulted in Papers I, II and III.
- Chapter 6 introduces the narrowband ultrasonic resonance spectroscopy technique and the contributions made in Papers IV, V and VI.
- Chapter 7 summarizes the conclusions .
- Chapter 8 suggests future work.

2. Lamb waves

2.1 Introduction

Isotropic elastic bulk media support two types of wave motion, longitudinal and shear. A longitudinal wave has its displacement in the direction of propagation, while a shear wave has its displacement perpendicular to the direction of propagation. These waves propagate with different velocities, where the velocity of the shear wave, c_S, is lower than the longitudinal wave's velocity, c_L.

Consider a harmonic *plane wave*, $s(x,t)$, propagating along the x-axis in a medium. Harmonic refers to a wave consisting of a single angular frequency, ω. Waves having constant phase over a plane, in this case perpendicular to the x-axis, are referred to as plane waves. The wave at position x and time t, can be described in complex form as

$$s(x,t) = Ae^{j(\omega t - kx)} \tag{2.1}$$

where k is the wavenumber and A is the amplitude of the wave. The wavenumber k is related to the phase velocity of the wave, c_p, as

$$k = \omega / c_p. \tag{2.2}$$

Henceforth, the harmonic dependency $e^{j\omega t}$ will be assumed implicitly for notational convenience.

The longitudinal and shear waves mentioned above both have frequency independent phase velocities, which results in linear frequency-wavenumber relationships. This means that these waves are non-dispersive and the shape of the waves will be preserved during propagation.

When the dimensions of the media approach the order of the wavelength, it starts behaving as a *wave guide*. Waves propagating in a wave guide are called *guided waves*. Such waves in infinite elastic plates were first described and analyzed by Horace Lamb in 1917, and they are therefore called *Lamb waves*. In application oriented publications, a commonly occurring name for guided waves in plates are *guided Lamb waves*. In contrast to bulk waves, guided waves are dispersive, i.e. they have frequency dependent dependent velocity. This means that the shape of a wave packet changes during propagation.

Another property Lamb waves shares with other types of guided waves is the possible existence of multiple propagation modes. These so called *Lamb modes* follow different dispersion relationships, i.e., the relation between phase velocity and frequency depends on the mode. As a consequence, there

may be several propagation velocities even for a single frequency. Depending on the thickness of the plate and the frequency of the wave, anywhere from two to infinitely many *Lamb modes* can propagate in the plate.

Compared to *Rayleigh waves*, which propagate in a shallow zone below the surface of a material, Lamb waves have through-thickness displacement permitting detection of defects both within and close to the surface of the plate. This, along with their ability to propagate over long distances, make them suitable for both inspection and monitoring of plate structures.

Beside Lamb waves, there is another type of guided wave modes in plates called shear horizontal (SH) modes [15]. These modes propagate with displacements in-plane, i.e. parallel to the plate, compared to Lamb waves which have only out-of-plane, i.e. perpendicular to the plate, components perpendicular to the direction of propagation. The SH-waves have not been given any special consideration in this work since the setup used for the experiments cannot detect this type of wave motion.

2.2 Basic model of propagating Lamb waves

Consider an isotropic homogeneous plate of thickness d illustrated in Figure 2.1. In this plate, harmonic waves of angular frequency ω can propagate in a number of Lamb modes. Let $c_{p,n}(\omega)$ denote the phase velocity of the n-th mode at ω, yielding the corresponding wavenumber $k_n(\omega) = \omega/c_{p,n}(\omega)$.

Consider now a line source producing a harmonic surface stress perpendicular to the plate at $u_3 = 0$, with u_3 indicated in the figure, and let $\overline{\mathcal{T}}(\omega)$ denote the amplitude of the stress. The excitation of mode n from the surface stress is modeled by the transfer function $\overline{H}_n(\omega)$. The normal displacement on the plate surface of the resulting wave propagating in the u_3 direction is then given by

$$U_n(\omega, u_3) = \overline{H}_n(\omega)\overline{\mathcal{T}}(\omega)e^{-jk_n(\omega)u_3}. \tag{2.3}$$

The total displacement at u_3 is given as a superposition of the modes

$$U(\omega, u_3) = \sum_n \overline{H}_n(\omega)\overline{\mathcal{T}}(\omega)e^{-jk_n(\omega)u_3}, \tag{2.4}$$

where the sum ranges over the possible modes at frequency ω.

The above scenario corresponds to a line source. A better representation of the small array elements considered in this work is to consider them as point-like sources. Such a source, producing an out-of-plane harmonic stress with amplitude $\mathcal{T}(\omega)$ at the origin, generates a cylindrical wave that will diverge radially as it propagates. Its displacement field can be approximated by

$$U(\omega, r) = \sum_n \frac{1}{\sqrt{r}} H_n(\omega)\mathcal{T}(\omega)e^{-jk_n(\omega)r}, \tag{2.5}$$

where r is the distance to the source. Note the difference in notation for the transfer function, $H_n(\omega)$, which indicates that a point source is considered.

The model (2.5) predicts how the out-of-plane displacement depends on the stress excitation and how it is affected by the distance r from the source. Note that in order to obtain $U(\omega, r)$ the dispersion characteristics, $k_n(\omega)$, has to be determined, as well as the number existing modes and the transfer function $H_n(\omega)$. The following sections will give a short introduction to these important properties of Lamb waves that are relevant to the work presented in this thesis.

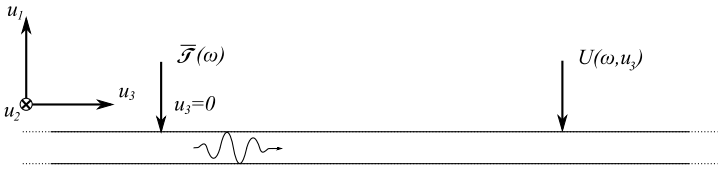

Figure 2.1: One dimensional plate model. A surface stress $\overline{\mathcal{T}}(\omega)$ normal to the plate excites propagating modes in the plate.

2.3 Rayleigh-Lamb equations

Consider again the plate introduced in the previous section with thickness d. Lamb modes can be either symmetric, i.e. with symmetric wave shapes across the plate thickness, or antisymmetric, i.e. with antisymmetric wave shapes. A wavenumber, k, of a possible propagating Lamb mode for a given frequency, ω, is a real solution to the Rayleigh-Lamb characteristic equations [15]

$$\frac{\tan(qd/2)}{\tan(pd/2)} = -\frac{4k^2pq}{(q^2-k^2)^2} \quad \text{for symmectric modes} \tag{2.6}$$

$$\frac{\tan(qd/2)}{\tan(pd/2)} = -\frac{(q^2-k^2)^2}{4k^2pq} \quad \text{for antisymmectric modes} \tag{2.7}$$

where $p^2 = (\omega/c_L)^2 - k^2$ and $q^2 = (\omega/c_S)^2 - k^2$, c_L is the longitudinal wave velocity and c_S is the shear wave velocity.

As mentioned earlier, for a given frequency there are typically several wavenumbers satisfying the Rayleigh-Lamb equations (2.6) and (2.7), each corresponding to a separate mode. For the lowest frequencies there are two solutions, the fundamental (anti-)symmetric $(\mathrm{A}_0)\mathrm{S}_0$ mode. The successive solutions for increasing frequencies, result in higher order modes. These are numbered $(\mathrm{A}_1)\mathrm{S}_1$, $(\mathrm{A}_2)\mathrm{S}_2$, and so forth. The frequency limit above which a particular mode can exist is called the mode's *cut-off frequency*. To allow a simple notation in equations a single index, $n = 0, 1, 2, 3, \ldots$, is used to identify modes $\mathrm{S}_0, \mathrm{A}_0, \mathrm{S}_1, \mathrm{A}_1, \ldots$, in this thesis.

The group velocity is the velocity at which the envelope of a narrowband wave packet propagates. It is related to the wavenumber as

$$c_g = \frac{d\omega}{dk}. \tag{2.8}$$

The group velocity provides insight into the amount of dispersion each mode is subjected to in various frequency bands. At frequencies where the group velocity changes sharply the wave is severely dispersed, while a frequency region with constant group velocity indicates low dispersion. As mentioned earlier, for non-dispersive media there is a linear relationship between the frequency and wavenumber, making the group velocity equal to the phase velocity $c_p = c_g$.

Figure 2.2 shows the phase and group velocities of the solutions to (2.6) and (2.7) for a 6 mm aluminium plate. Its material properties correspond to a plate used in the experiments presented in Paper I–III. The effect of dispersion is illustrated in Figure 2.3. A bandpass filtered 1 cycle 300 kHz sinusoidal stress at $u_3 = 0$, shown in the first plot, is used to simulate propagation of two modes, S_0 and A_0, in a 6 mm Al plate using (2.4). For simplicity it is assumed that both modes are excited equally, that is, $\overline{H}_0(\omega) = \overline{H}_1(\omega)$. The wavenumbers, $k_n(\omega)$, used for the simulation are given by the dispersion characteristics in Figure 2.2. The frequency band between the dash-dot lines is the bandwidth of the signal. The plots in the lower part of Figure 2.3 show the surface displacement at distances 0.2 and 0.4 m. It can be seen that the S_0 mode is severely dispersed, while the shape of the A_0 mode is only slightly altered by the propagation. This can be explained by observing in Figure 2.2 that the group velocity of the A_0 mode is almost constant in the frequency band of the signal.

2.4 Lamb wave excitation and detection

Most of the work on plate inspection using Lamb waves relys on concepts assuming a single dominant mode which enables estimation of time-of-flight and beamforming without significant interference from other Lamb modes. This work has depended on the development of transducers and instrumentation that are mode selective.

Perhaps the simplest way of exciting a single Lamb mode is by generating an ultrasonic wave with a suitable angle of incidence into the plate [15], which is the basic principle of *angle beam transducers*. Angle beam transducers consist of a transducer and a plastic wedge that gives the generated waves a particular incidence angle to the plate, resulting in a directional wave. The angle of the incident wave and its frequency determine the amplitudes of the excited modes, and can therefore enable mode selectivity [15]. The amplitudes of excited Lamb modes are in general frequency dependent and highly

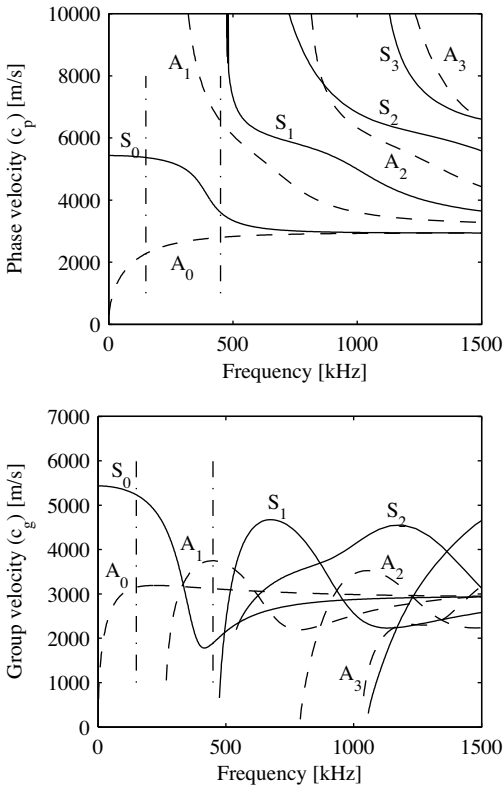

Figure 2.2: Dispersion curves for 6 mm Al plate. Phase velocity (top) and group velocity (bottom). Dash-dot lines show the frequency band of the signal in Figure 2.3.

affected by the transducer type. This is the reason for using mode and source dependent transfer functions $H_n(\omega)$ and $\overline{H}_n(\omega)$ in Section 2.2, as the excitation will couple to various modes differently. For instance, a small transducer may be approximated by a point source. Other transducers may be better approximated using line sources. The analytic expressions required to calculate the transfer functions can be found in, for example, [16, 15, 17].

An alternative to angle beam transducers are interdigital transducers (IDT). These transducers consist of finger shaped metallic coatings on a piezoelectric substrate as in a surface acoustic wave (SAW) device. The wavelength of the resulting Lamb wave is determined by the distance between the fingers of the transducer and the input signal frequency. Experimental work evaluating the use of IDTs for Lamb wave generation and reception include [18, 19, 20]. Since these transducers generate highly directional waves they are not suitable for applications where omni-directional coverage is desired.

Omni-directional mode selectivity requires different methods. For array applications, Wilcox used a circular array of EMAT transducers to excite an

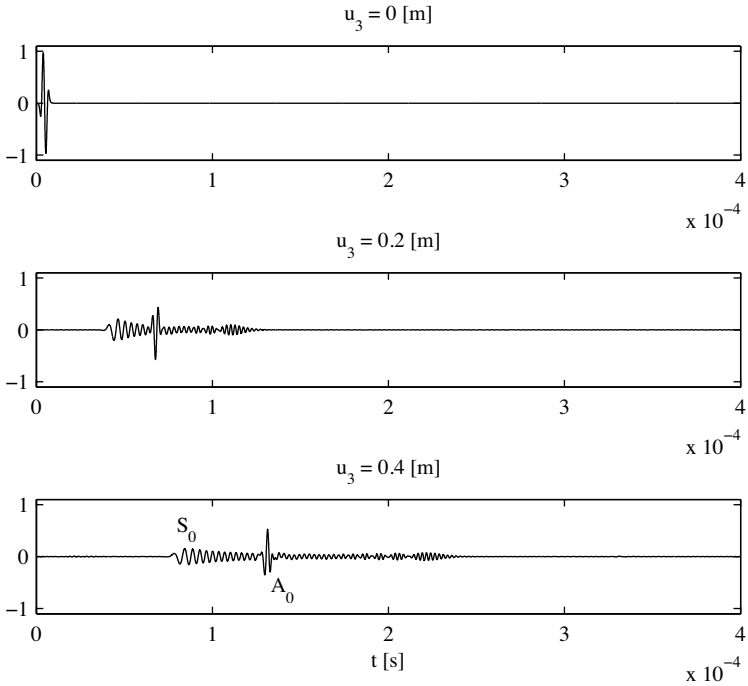

Figure 2.3: Normal surface displacement at various distances when the excitation signal is a bandpass filtered 300 kHz 1 cycle sinusoid. Two modes are simulated, the S_0 and A_0 mode having equal power. The A_0 mode is almost non-dispersed whereas the S_0 mode is severely dispersed.

omni-directional S_0 mode [21, 22]. In [23], Giurgiutiu proposed an approach where the size of piezoelectric elements was selected to improve the mode selectivity for a certain frequency range.

In summary, most important in these methods is frequency selection to achieve mode selectivity, which comes at the price of limited bandwidth. As a consequence, a design relying on this idea may yield signals that have too poor range resolution for certain applications. This may hold for instance in imaging applications. As discussed in Section 2.3, the choice of frequency also affects the dispersion of the wave packet. Thus, there is a trade-off between mode selectivity and low dispersion, and bandwidth. However, using a transducer that is mode selective in a low dispersive frequency band simplifies direct interpretation of the received signals.

For more information concerning different transducer techniques for Lamb wave generation and detection see the review articles [3, 13, 14], and the references therein.

2.5 Experimental estimation of dispersion characteristics

It should be apparent from the discussions in the previous sections, that the dispersion characteristics play an important role in plate inspection using Lamb waves.

To take dispersion into account and achieve sufficient performance in range estimation, accurate estimates of the dispersion characteristics of the structure are required. The adaptive beamforming approaches considered in this work are particularly sensitive to errors in phase velocity, see Section 3.9.

For homogeneous isotropic structures it may be sufficient to solve the Rayleigh-Lamb equations in (2.6) and (2.7), using estimates of the bulk wave velocities. More complex structure consisting of, for example, anisotropic materials or multiple layers, may require a more direct approach to the estimation of the dispersion characteristics. Several approaches have been presented for experimental determination of the the frequency dependent phase velocities of multimodal Lamb waves.

Alleyne and Cawley [24] proposed an approach using a two dimensional FFT on signals received at regular distances from a broadband source to estimate the wavenumbers for each frequency. By first performing a temporal FFT on each of the received signals, followed by a spatial FFT over the recevied signals for each frequency, their method results in a frequency-wavenumber spectrum.

An example of this estimation for the 6 mm Al plate, used in Papers I–III, can be seen in Figure 2.4. The experimentally estimated dispersion curves for the different modes are clearly seen and can be compared to the theoretical curves by presenting the solutions in Figure 2.2 as wavenumbers instead of phase velocities, $k = \omega/c_p$.

Other approaches for estimating dispersion characteristics include time-frequency analysis, such as the short-time Fourier transform (STFT). Such methods allow the phase velocities for the different modes to be estimated using a broadband source and a single receiver at fixed positions. Some of these methods are reviewed and evaluated by Niethammer et al. [25].

2.6 Scattering and reflection of Lamb waves

When performing inspection using ultrasound in, for example, a pulse-echo or pitch-catch setup, the presence and amplitude of the reflected or transmitted signals provide valuable information concerning the state of the object. Unfortunately, for Lamb waves the reflection at boundaries are often very complicated compared to, for example, bulk waves. Both naturally occurring boundaries, such as plate edges or welds, and defects, such as corrosion pits or cracks, may affect the shape of the wave on reflection. One reason for this

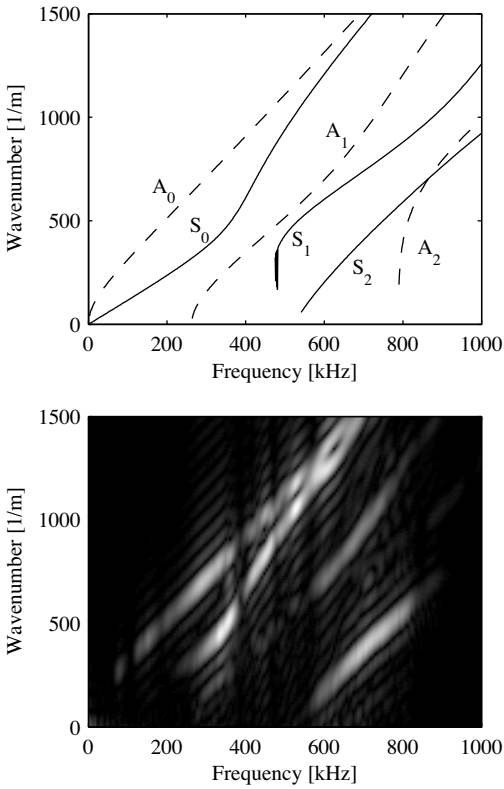

Figure 2.4: Dispersion curves for 6 mm Al plate used in the experiments. Theoretical (top) and experimental (bottom) frequency-wavenumber spectra.

is that the reflection and transmission coefficients are frequency dependent for many types of discontinuities [10, 26]. Furthermore, depending on the characteristics of the boundary and the frequency content of the Lamb wave, mode conversion could occur between modes of different order, e.g. A_0 to A_1, as well as between antisymmetric and symmetric modes [15]. Recall from Section 2.4 that the initial wave generated by a transmitter can consist of multiple modes that, on reflection, are split into even more modes and hence the received wave becomes more complex. An important consequence of this is that methods used for detection or estimation of Lamb waves have to be robust with respect to variations in the shape of the wave. Detailed studies of the mode conversion phenomenon at, for example, plate edges can be found in [27], and for notches in [28, 29].

Mode conversion at defects could, if handled correctly be used as a source of information, and should therefore not be seen purely as a problem. In for example [26, 30], the presence of converted modes was proposed to indicate a

defect. The amplitude of a converted mode was also used to estimate the size of cracks.

2.A Dispersion compensation

Knowledge of the dispersion characteristics for a particular mode enables straightforward compensation of the dispersive effects from propagation for that mode. This can allow a wider bandwidth of the signals as long as sufficient mode selectivity can be achieved. In [31], Wilcox provides a thorough analysis of basic dispersion compensation and also proposes a computationally efficient approach to the problem.

The most straightforward way of compensating is to simply phase shift each frequency component corresponding to a certain propagation distance. This can be performed for a distance z at $t = 0$ as

$$h(z) = \int_{-\infty}^{\infty} G(\omega) e^{jk_n(\omega)z} \mathrm{d}\omega. \tag{2.9}$$

where $G(\omega)$ is the Fourier transform of a dispersed signal. Assuming that $t = 0$ was the excitation time, this has removed the dispersion by backpropagating the signal to its initial position.

The direct calculation of the integral in (2.9) for each distance is computationally demanding. In [31] Wilcox used the inverse FFT to transform data from wavenumber domain into the spatial domain. Since the frequency-wavenumber relationship is non-linear in the dispersive case, the frequency domain data needs to be interpolated into equally spaced wavenumber points before applying the inverse FFT. This approach is of course computationally much more efficient.

3. Beamforming

3.1 Introduction

Beamforming is the concept of forming directional beams using an aperture. For example, the dish of a satellite antenna provides directionality by reflecting energy from a specific direction to the head, which contains the actual antenna. To receive signals from other directions, mechanical steering of the dish is required.

In radar, directional steering can be achieved by rotation of the antenna allowing scanning of one direction at a time. Being an active technique, which both transmits and receives data, it is capable of range resolution. For other applications mechanical steering might be impractical and sometimes impossible. For SHM or NDT a much more convenient alternative would be to use arrays of sensors, which enable electronic steering of the received signals.

Arrays usually consist of a set of identical transducers, although transmitting and receiving array elements can be of different types. An active setup can be of basically any geometry and combination of transmitting and receiving elements as seen in Figure 3.1. It is also common that the instrumentation is capable of switching between transmission and reception of the elements during a single excitation cycle to both transmit and receive using the same element.

In array imaging, one or several transmitters are excited using a probing signal, in this thesis an elastic wave, which is transmitted into the object. The propagating elastic wave is reflected at boundaries, such as defects, and those reflections are received by the array. Knowledge of the position of the transmitter, the instant of excitation, and the phase velocity in the material enables both angle and range estimation. The backscattered data is then processed to reconstruct an image of the internals of the object in the region-of-interest (ROI).

It is worth noting that for inspections using active setups, where the excitation and reception procedure can be repeated indefinitely, the array is merely a convenience. The key to the processing algorithms is the spatially distributed measurement positions of the array that allow spatial resolution. For a stationary environment there is nothing in the actual processing step preventing the acquisition to be performed sequentially by manual positioning of two transmitting/receiving elements on a set of points forming a virtual array.

A dataset of backscattered signals acquired using a single transmission will be referred to as a *single snapshot*. When a dataset is acquired using separate

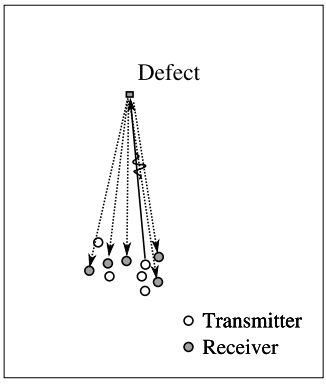

Figure 3.1: General setup for array imaging of plates. The acquisition is repeated for each transmitting element.

transmissions from multiple spatial position, such as an array of transmitting elements, it will be referred to as *multiple snapshot*. This distinction will be important in the discussion on correlated signals in Section 3.8.

3.2 Standard beamforming

The simplest and most widely used technique for beamforming is the delay-and-sum (DAS) beamformer, or simply, the standard beamformer. Its principles are simple; by applying delays on the received data from each receiver element prior to summation, the output from the beamformer can be steered in a certain direction. Signals impinging from the steered direction will add up constructively, while interfering signals from other directions will generally be reduced. This is referred to as *coherent* averaging of signals from the steered direction.

A typical array setup is illustrated in Figure 3.2 for a so-called uniform linear array (ULA). A ULA is a linear array with equispaced array elements. The figure illustrates a plane wave, $s(t)$, impinging on the array. The resulting signals acquired from each element are shown in Figure 3.3.

Let $g_m(t)$ denote the signal received by element m. All signals received by the array can be ordered in a column vector $\mathbf{g}(t)$ as

$$\mathbf{g}(t) = \begin{bmatrix} g_0(t) & g_1(t) & \cdots & g_{M-1}(t) \end{bmatrix}^T. \tag{3.1}$$

In this example element 0 is used as a reference and it receives the signal $g_0(t) = s(t - T)$, where T is a time delay. Element 1 receives the signal τ_1 seconds later, $s(t - T - \tau_1)$. Element 2 receives $s(t - T - \tau_2)$, etc. To steer the array to the direction of the signal, each channel m has to be time-shifted by τ_m s, which corresponds to the delay caused by the time-of-flight between

the elements for a particular direction θ. The delayed and aligned signals are shown in Figure 3.3. This is beamforming on reception, but the same concept also allow steering of transmitting signals. Steering on transmission will direct the transmission power to a particular direction.

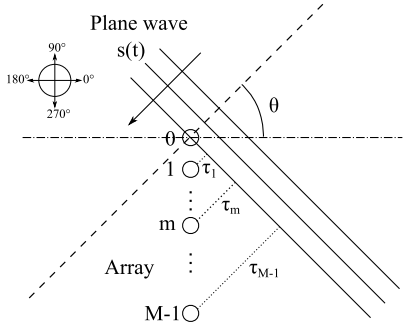

Figure 3.2: Plane wave impinging on a ULA from direction θ. Element 0 is used as reference position.

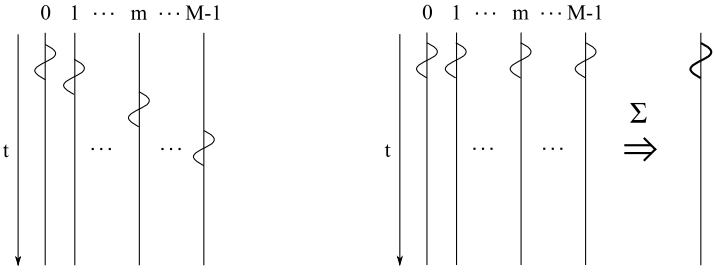

Figure 3.3: Left: The signals received by each array element. Right: Applying time-shifts aligns signals from a particular direction before summation.

In general, the receivers will pick up signals from several directions simultaneously. If θ is the direction of current interest, the signals arriving from other directions are considered as interfering signals and the corresponding sources are often called interferers. Moreover, the acquired signals are typically noise corrupted, with the noise sources being, for instance, thermal noise in the electronics. In array processing it is common to define the measure signal-to-interference and noise ratio (SINR)

$$\mathrm{SINR} = \frac{P_{\mathrm{signal}}}{P_{\mathrm{noise}} + P_{\mathrm{interference}}}, \tag{3.2}$$

where P denotes the power of the respective components.

Steering the transmitted signal improves the SINR for potential reflectors in the steered direction. Reflected signals from the steered direction will have

higher amplitudes, which will improve the signal-to-noise ratio (SNR) in the electronics. A disadvantage with this is that the focused transmission has to be repeated for all angles in the ROI. These datasets are often processed independently using DAS.

An alternative to steering on transmission is to excite each transmitter separately and acquire multiple snapshots of backscattered signals. This dataset can then be used for *synthetic focusing* during post-processing by performing a DAS operation on the data from each transmission and average the results. This will improve the SINR, however, since the noise level of the receiving electronics is fairly independent of the signal level, acquiring backscattered signals from single excitations results in lower SNR compared to when steering on transmission. Furthermore, detection of small amplitudes may also be limited by the dynamic range of the AD-converters in the receiver.

3.3 The array steering vector

For narrowband signals[1] the delays can be implemented as simple phase-shifts, allowing a simple mathematical description through the so called *array steering vector* or *array manifold vector*, which is the most fundamental mathematical model of an array.

The steering vector consists of phasors corresponding to the relative phase-shifts for each array element related to the propagation over the array for a plane wave impinging from a particular direction.

Thus for narrowband signals with center frequency ω, the steering vector for a M element ULA can be written as

$$\mathbf{a}(\theta) = \begin{bmatrix} 1 & e^{-j\omega\tau_1(\theta)} & \cdots & e^{-j\omega\tau_{M-1}(\theta)} \end{bmatrix}^T, \tag{3.3}$$

where $\tau_m(\theta)$ is the relative propagation time for signals from angle θ, where element 0 is used as a reference.

For a M element ULA with element spacing d, the exponential for each element m is given by

$$\omega\tau_m(\theta) = mkd\sin\theta, \tag{3.4}$$

where k is the wavenumber. Insertion in (3.3) gives

$$\mathbf{a}(\theta, k) = \begin{bmatrix} 1 & e^{-jkd\sin\theta} & \cdots & e^{-j(M-1)kd\sin\theta} \end{bmatrix}^T. \tag{3.5}$$

For most traditional applications, the wavenumber is directly given by frequency and is therefore usually omitted as a parameter for narrowband sig-

[1] A narrowband signal can be modeled as $\mathrm{Re}\{\tilde{s}(t)\exp(j\omega t)\}$, where $\tilde{s}(t)$ is a slowly varying complex envelope. Slowly varying in this case means that it can be considered constant during the propagation over the array.

nals, as $\mathbf{a}(\theta)$. Recall from Chapter 2 that Lamb waves are multimodal with the possibility of multiple wavenumbers for each frequency component. Therefore, in order to separate different modes, a 2D wavenumber is used to represent an impinging signal, $\mathbf{k} = [k_x, k_y]^T$, or in polar coordinates (θ, k), where $k_x = k\cos(\theta)$ and $k_y = k\sin(\theta)$.

Using the steering vector, a model of the received narrowband signals $\mathbf{g}(t)$ can be written as

$$\mathbf{g}(t) = \mathbf{a}(\theta, k)s(t) + \mathbf{n}(t), \tag{3.6}$$

where $\mathbf{n}(t)$ is a superposition of noise and potential interferers. The steered output for narrowband signals can be written as

$$y(t) = \frac{1}{M}\mathbf{a}^H(\theta, k)\mathbf{g}(t) \tag{3.7}$$

where ^{H} is the conjugate transpose, and M normalizes the output to unit gain for the steered direction.

The effect of the beamforming operation becomes obvious when inserting (3.6) into (3.7)

$$\begin{aligned} y(t) = \frac{1}{M}\mathbf{a}^H(\theta, k)\mathbf{g}(t) &= \frac{1}{M}\mathbf{a}^H(\theta, k)\left(\mathbf{a}(\theta, k)s(t) + \mathbf{n}(t)\right) \\ &= s(t) + \frac{1}{M}\mathbf{a}^H(\theta, k)\mathbf{n}(t), \end{aligned} \tag{3.8}$$

using that $\mathbf{a}^H(\theta, k)\mathbf{a}(\theta, k) = M$. Hence, the output of the beamformer is $s(t)$ plus the contribution from the incoherently averaged noise and interference.

It is necessary to make a distinction between sources that can be considered as near the array, and sources far from the array. A signal originating from the vicinity of the array, can be considered as *near-field* if the propagating wave has a curved wavefront. This means that the phase delays between the array elements are not only a function of angle, but also of range. Sources further away from the array are in the far-field if the impinging wave has a plane wavefront, a *plane wave*, making the phase delays between the array elements approximately functions of only angle. This is particularly important when using adaptive algorithms in near-field as described in Chapter 5.

3.4 Array and beam pattern

The standard beamformer described above does not allow perfect isolation of signals from a particular direction. That is, signals outside the steering angle can cause significant interference. An important tool in characterizing the performance of an array is the *array pattern*. It is the output of an unsteered

standard beamformer for incoming plane waves of unit amplitude over a range of angles and wavenumbers.

A general and simple expression for the array pattern for an unweighted array is [32]

$$\mathcal{A}(\mathbf{k}) = \frac{1}{M} \sum_{m=0}^{M-1} e^{j(k_x x_m + k_y y_m)}, \tag{3.9}$$

where M is the number of elements in the array, (x_m, y_m) is the position of element m, and $\mathbf{k} = [k_x, k_y]^T$ is the wavenumber vector in Cartesian coordinates.

Closely related to the array pattern is the *beampattern*. The beampattern is the output power of a beamformer steered to a particular direction for signals impinging from a range of angles for a *fixed* wavenumber magnitude. This is particularly useful when analyzing narrowband single-mode signals.

An example of a beampattern of an 8 element ULA steered to 0° is shown in Figure 3.4. The element spacing is set to half the wavelength. In the center of the plot is the *main lobe*. The width of the main lobe is a measure of the angular resolution and affects the ability to resolve closely spaced sources. The other lobes are called *sidelobes*. The height of the lobes shows how much a unit amplitude interferer from each angle will contribute to the output. Note that at certain angles this contribution is zero, which is referred to as a *null* in that direction.

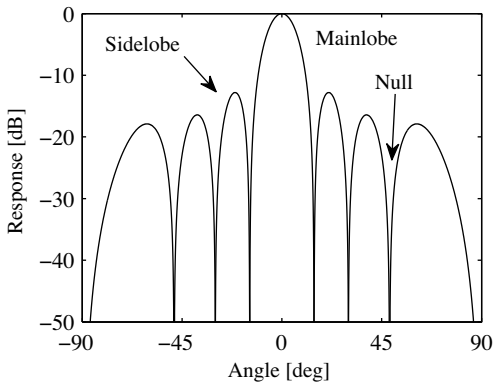

Figure 3.4: Beampattern of an 8 element ULA, with an element spacing equal to half the wavelength of the impinging signal.

The beampattern can be altered by weighting signals received by the array elements differently[2]. Using standard window functions, such as the Hamming window, as array weightings leads to a beampattern with lower sidelobes, at the cost of lower resolution. A more general expression for the beam-

[2]This is called apodization or shading.

former in (3.7) is

$$y(t) = \mathbf{w}^H \mathbf{g}(t). \tag{3.10}$$

The weight vector $\mathbf{w}$ for a standard beamformer using apodization is simply the weighted steering vector

$$\mathbf{w} = \frac{1}{M}\begin{bmatrix} w_0 & w_1 e^{-jkd\sin\theta} & \cdots & w_{M-1}e^{-j(M-1)kd\sin\theta}\end{bmatrix}^T \tag{3.11}$$

where w_m is given by the window function. Thus, the weight vector $\mathbf{w}$ depends on the angle θ which will be implicitly assumed in the following text.

Considering again the array in Figure 3.4, Figure 3.5 shows the beampattern of the 8 element ULA with Hamming window apodization. The sidelobes are significantly lower, while the mainlobe is much wider leading to worse resolution.

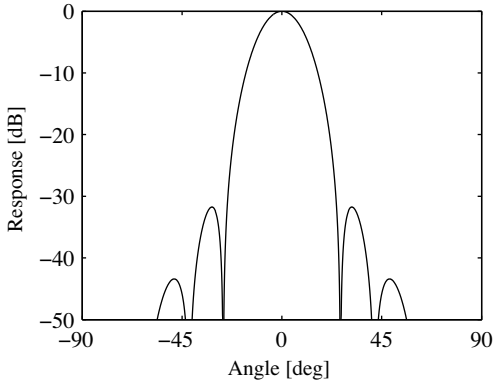

Figure 3.5: Beampattern of an 8 element ULA with Hamming window apodization.

Different techniques have been proposed to design beampatterns based on different criteria. For example, the Dolph-Chebychev technique yields the narrowest mainlobe for a given constant sidelobe level [33]. Note that these approaches are independent of the actual signal and interference environment. If the directions of actual interferers where known, or could be estimated, it would be possible to design a beampattern with nulls at these angles, and allow high sidelobes at angles without interference. This type of approaches are called *adaptive beamformers*.

3.5 Minimum variance distortionless response

One of the most common adaptive beamformers is the minimum variance distortionless response (MVDR) beamformer. The MVDR approach has its

origins in frequency-wavenumber estimation of seismic waves. It was proposed by Capon [34] and has therefore also been called Capon's maximum likelihood method or simply Capon's method.

The MVDR beamformer is derived under the assumptions of somewhat idealized conditions. In the ideal case, second-order statistics of a stationary noise and interference environment are available. These second-order statistics are in the form of the noise covariance matrix,

$$\mathbf{R}_{ni} = \mathrm{E}\left[\mathbf{g}_{ni}(t)\mathbf{g}_{ni}^{H}(t)\right] \tag{3.12}$$

where $\mathbf{g}_{ni}(t)$ is the noise and interference data received by the array, and E denotes the expected value. The noise covariance matrix can be exploited by the MVDR approach to maximize the SINR, defined in (3.2).

The MVDR weight vector is designed based on the following criterion: minimize the expected output power of the noise and interference $P_{ni} = P_{\text{noise}} + P_{\text{interference}}$, while signals from the steered direction, θ, having wavenumber k, are passed undistorted.

For a given weight vector, $\mathbf{w}$, the noise output power

$$P_{ni} = \mathrm{E}\left[|\mathbf{w}^{H}\mathbf{g}_{ni}(t)|^{2}\right] = \mathrm{E}\left[\mathbf{w}^{H}\mathbf{g}_{ni}(t)\mathbf{g}_{ni}^{H}(t)\mathbf{w}\right] = \mathbf{w}^{H}\mathbf{R}_{ni}\mathbf{w}, \tag{3.13}$$

where $\mathbf{R}_{ni}$ is defined in (3.12).

The MVDR weight vector is thus defined as

$$\mathbf{w}_{\text{MVDR}} = \arg\min_{\mathbf{w}} \mathbf{w}^{H}\mathbf{R}_{ni}\mathbf{w} \tag{3.14}$$

under the constraint

$$\mathbf{w}_{\text{MVDR}}^{H}\mathbf{a}(\theta, k) = 1. \tag{3.15}$$

The solution to this optimization problem is found through the use of Lagrange multipliers, and can be written in closed form as [35]

$$\mathbf{w}_{\text{MVDR}} = \frac{\mathbf{R}_{ni}^{-1}\mathbf{a}(\theta, k)}{\mathbf{a}^{H}(\theta, k)\mathbf{R}_{ni}^{-1}\mathbf{a}(\theta, k)}. \tag{3.16}$$

Unfortunately, the noise statistics are rarely available. Estimation of the noise covariance matrix would require the noise and interference to be measurable without the actual signal. The noise covariance matrix is therefore often replaced by the signal covariance matrix,

$$\mathbf{R} = \mathrm{E}\left[\mathbf{g}(t)\mathbf{g}^{H}(t)\right], \tag{3.17}$$

again assuming a stationary environment. The signal covariance matrix can be estimated as

$$\widehat{\mathbf{R}} = \frac{1}{N_s}\sum_{t=1}^{N_s}\mathbf{g}(t)\mathbf{g}^{H}(t), \tag{3.18}$$

with N_s being the number of samples used for the estimate. The resulting MVDR weight vector using the estimated covariance matrix (3.18) is given by

$$\mathbf{w}_{\text{MVDR}} = \frac{\widehat{\mathbf{R}}^{-1}\mathbf{a}(\theta,k)}{\mathbf{a}^H(\theta,k)\widehat{\mathbf{R}}^{-1}\mathbf{a}(\theta,k)}. \tag{3.19}$$

In non-stationary environments it may be necessary to estimate the covariance matrix using only a few samples. If the number of samples N_s is less than the number of array elements M, the covariance matrix will not have full rank and is therefore non-invertible. Sections 3.8 and 3.9 discuss some options to improve the rank of the covariance matrix and to make it invertible.

Note that the use of the signal covariance matrix[3] in (3.17) or (3.18), instead of the noise covariance matrix, (3.12), leads to some issues that will be addressed in Sections 3.8 and 3.9.

3.6 2D array configurations

Although arrays can have any number of elements in any topology, the most common array configurations have standard geometrical shapes. The array configuration most familiar, and intuitively understandable, is probably the ULA in which the elements are regularly spaced along a line. For applications requiring 360° coverage, the ULA has two significant drawbacks. Firstly, its resolution is highly angle dependent. Secondly, it has a front-back ambiguity making it impossible to discriminate signals impinging from the back and front of the array, which limits the usable angular coverage to 180°. This motivates the use of 2D arrays that do not suffer from this ambiguity. Common 2D array topologies include circular and rectangular arrays, which will be briefly described below.

A uniform circular array (UCA) consists of a number of array elements uniformly distributed on a circle as illustrated in Figure 3.6. The array steering vector for an M element UCA with radius R can be written as

$$\mathbf{a}(\theta,k) = \Big[e^{jkR\cos(\theta)} \quad e^{jkR\cos(\theta-\gamma_c)} \quad \cdots \quad \cdots \quad e^{jkR\cos(\theta-(M-1)\gamma_c)}\Big]^T, \tag{3.20}$$

[3] In some work, such as [33], the signal covariance matrix approach is named the minimum power distorionless response (MPDR), and MVDR is reserved for the noise covariance matrix approach. Other naming conventions can also be found. In the works referenced in this thesis the term MVDR, or minimum variance, is used even though the signal covariance matrix is used. This convention is also used in this thesis.

where $\gamma_c = 2\pi/M$ is the separation in angle between the elements, k the wavenumber and θ the incident angle. An important feature of the UCA is that it has a beampattern that is practically angle independent.

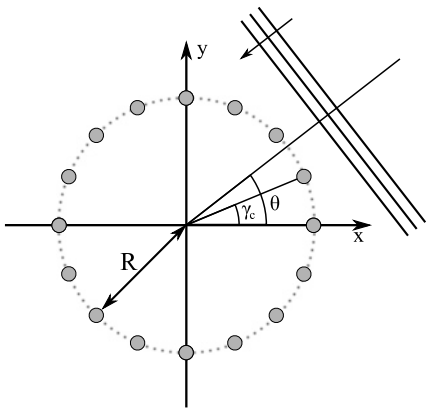

Figure 3.6: A uniform circular array (UCA).

The last array configuration to be introduced is the uniform rectangular array (URA). A URA consists of elements ordered in M_r equispaced rows and M_c columns. The steering vector for a URA, having element spacing d, as illustrated in Figure 3.7, with the columns and rows distributed in the x-, and y-directions, respectively, can be set up by stacking steering vectors corresponding to rows of ULAs [33]. Here, Cartesian coordinates are used for convenience. Let the steering vector for row m_r be

$$\mathbf{a}_{m_r}(k_x, k_y) = \Big[e^{jm_r k_y d} \quad e^{j(k_x d + m_r k_y d)} \quad \dots \quad \dots \quad e^{j((M_c-1)k_x d + m_r k_y d)} \Big]^T, \quad (3.21)$$

where k_x and k_y are the wavenumber components in the x- and y-direction, respectively, and d is the element spacing. The stacked steering vector then takes the following form

$$\mathbf{a}(k_x, k_y) = \begin{bmatrix} \mathbf{a}_0(k_x, k_y) \\ \vdots \\ \mathbf{a}_{M_R-1}(k_x, k_y) \end{bmatrix}. \quad (3.22)$$

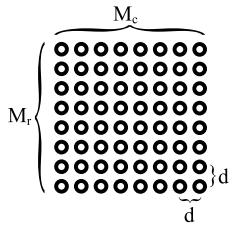

Figure 3.7: A uniform rectangular array (URA).

3.7 Spatial aliasing

Analogous to the sampling theorem for acquisition of temporal signals, spatial sampling requires the distance between the sampling positions to be sufficiently small compared to the wavelenght of the signals to avoid aliasing. In beamforming, spatial aliasing manifests itself as the appearance of replicas of a signal from one or several other directions than the true signal, making the true direction of the signal ambiguous.

In the beampattern, lobes will appear at the angles corresponding to the false directions. For a ULA or URA, these lobes, which are referred to as grating lobes have, in contrast to sidelobes, amplitudes equal to the main lobe. This occurs when the distance between the array elements is larger than half-wavelength of the signal.

To begin with a simple example, spatial aliasing is illustrated using the beampatterns of two ULAs in Figure 3.8. The arrays have equal width, but different element distance and thus different number of elements. The top plot shows the beampattern of an array with half-wavelength interelement distance, and the bottom plot of an array with one wavelength interelement distance. The true signal impinge from 45°, which is correctly shown in the top plot. The bottom plot, on the other hand, has a second, aliasing, lobe at -17°, which is due to the undersampling of the array. This leads to an ambiguity of the direction of the true signal.

UCAs have a more complicated array pattern compared to ULAs or URAs. Figure 3.9 shows the array pattern of a UCA having 16 uniformly distributed elements and a diameter of 40 mm. In the figure there are no replicas of the main lobe, but several slightly lower grating lobes appear above 800 rad/m. The maximum wavenumber allowed is related to the distance to the closest grating lobes.

To explain how these grating lobes cause aliasing, it is necessary to see how the array pattern interacts with the impinging signals. The array pattern acts as a smoothing function through convolution with the wave field [32]. Consider first a scenario where an incoming signal with wavenumber 300 rad/m impinge from 0°, which in Cartesian coordinates is $\mathbf{k}_s = (300, 0)$. Such a wave field can be represented by a Dirac function, $\delta(\mathbf{k} - \mathbf{k}_s)$, in the wavenumber

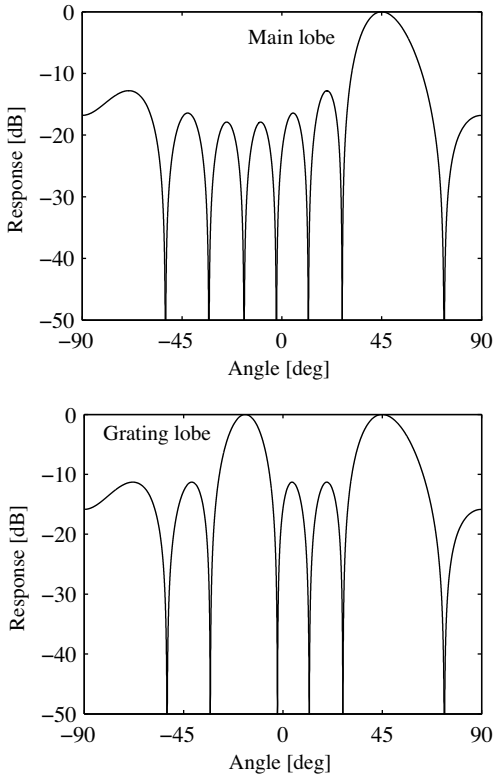

Figure 3.8: Beam patterns of two 8 element ULAs for a signal impinging from $45°$. The top plot for a ULA that is not under-sampled. The bottom plot for an under-sampled array where a grating lobe appears at $-17°$.

domain. Assume now that the input direction and wavenumber of the impinging signal is sought. The so called *steered response* of an array, is the output of a beamformer when steered to a range of wavenumbers for a fixed wave field. The steered response is given by

$$\mathcal{A}(\mathbf{k}) * \delta(\mathbf{k} - \mathbf{k}_s) = \mathcal{A}(\mathbf{k} - \mathbf{k}_s) = \frac{1}{M} \sum_{m=0}^{M-1} e^{j((k_x - 300)x_m + k_y y_m)}, \quad (3.23)$$

where $*$ denotes convolution.

The upper part of Figure 3.10 shows the resulting steered response for a range of wavenumbers. It can be seen that the true wavenumber and angle of the signal can be unambiguously determined if the the wavenumber range is limited to ≤ 400 rad/m, which is called the *visible region*, shown within the solid circle in the figures.

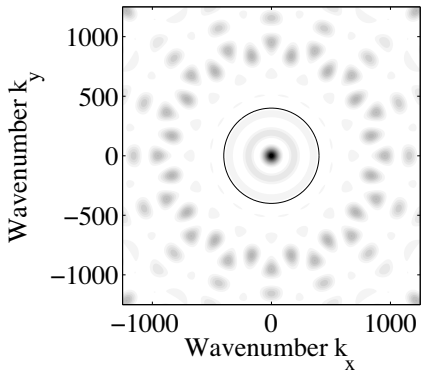

Figure 3.9: Array pattern of the 16 element UCA with a 40 mm diameter. Solid circle indicates the visible region. Linear 16 level contour plot.

Consider now an incoming signal with wavenumber 600 rad/m, impinging from $0°$. The resulting steered response is shown in the lower part of Figure 3.9. The true wavenumber is now outside the visible region. However, grating lobes have entered the visible region on the opposite side of the array. This will appear as several imping signal from a different direction and at different wavenumbers. To avoid that the grating lobes enter the visible region, the maximum wavenumber allowed is approximately 400 rad/m, or half the distance to the closest grating lobe. This allows unambiguous detection of signals within the visible region.

Two things can be noted: Firstly, if the signals are known to impinge from $-90° \leq \theta \leq 90°$, the aliasing peaks will not be ambiguous. Secondly, the grating lobes can be considered as "false" grating lobes in the sense that they are not replicas of the main lobe and have lower amplitude, cf. the grating lobes for ULAs. Thus the steering vector corresponding to one of these lobes is not identical to the steering vector for signals arriving from that angle and wavenumber. In Paper I this is exploited by the MVDR approach, which is able to suppress these grating lobes.

3.8 Correlated signals

This section returns to the issues mentioned in Section 3.5 concerning the use of the signal covariance matrix instead of the noise covariance matrix in the MVDR approach. Many advanced array processing methods require, in their standard form, that the impinging signals are uncorrelated. However, for array approaches using active excitation, the backscattered signals are naturally highly correlated. Correlated sources may result in so-called signal cancellation [36], which causes the true signal to be suppressed and spatially per-

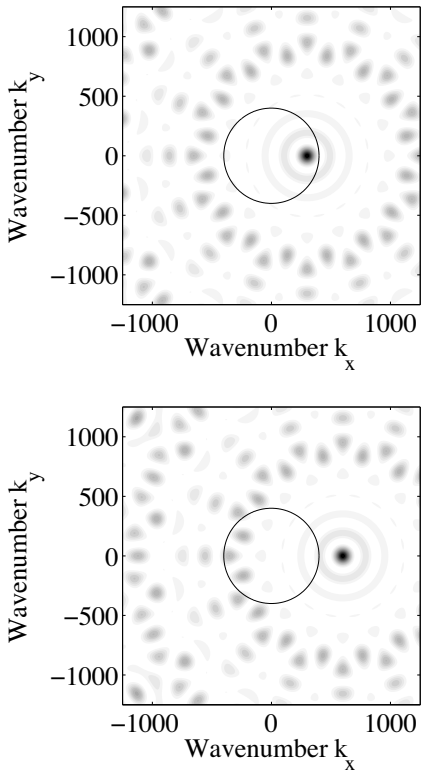

Figure 3.10: Steered responses of the 16 element UCA with a 40 mm diameter for impinging signals from $0°$ with wavenumbers 300 rad/m (top) and 600 rad/m (bottom). Solid circle shows the visible region. The bottom plot shows grating lobes within the visible region.

turbed by the beamformer. This has likely been one of the reasons preventing widespread use of more sophisticated methods, for example, adaptive beamformers in active array applications.

For a passive array, or an active setup with only one transmitter, the MVDR approach requires preprocessing to decorrelate correlated signals. Two examples of such methods are the *coherent subspace approach* [37], and *spatial smoothing* [38]. Previous work on imaging in sonar [39] and medical imaging [40, 41] have shown good results using the spatial smoothing approach. This section will therefore present an overview of that concept.

Spatial smoothing can be applied on array geometries that can be divided into a set of identical subarrays, for example ULAs or URAs. The idea is to estimate covariance matrices for each of the subarrays and then average them into a spatially smoothed covariance matrix.

An array configuration relevant to this work is the URA. The spatial smoothing of a URA is performed by dividing the array into L rectangular subarrays, see Figure 3.11. The covariance matrices estimated using data from each of the subarrays, l, are then averaged forming a spatially smoothed covariance matrix

$$\widehat{\mathbf{R}} = \frac{1}{L}\sum_{l=1}^{L}\widehat{\mathbf{R}}_l, \tag{3.24}$$

where $\widehat{\mathbf{R}}_l$ is the covariance matrix for subarray l estimated using, e.g., (3.18).

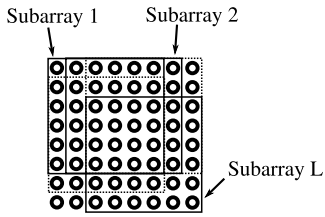

Figure 3.11: URA divided into L subarrays.

Besides the requirement on array geometry, dividing the array into smaller subarrays reduces the effective aperture size to that of the subarrays. However, for multiple snapshot data, these problems can be avoided. Covariance matrix estimates can be calculated using the received data from each transmission. Averaging those matrices have the same affect as averaging over the subarray covariance matrices for spatial smoothing, but with preserved aperture size. This approach was used by Wang [42] for medical ultrasound imaging.

The use of either spatial smoothing or multiple snapshot data, for covariance matrix averaging, reduces the need for temporal averaging as in (3.18). Temporal averaging may not produce the desired result in non-stationary environments, cf. Section 3.10.

3.9 Robustness against parameter uncertainties

Another issue related to the use of the signal covariance matrix is poor robustness. In practice there are always uncertainties in parameters, such as, phase-velocity and array element positions, leading to errors in the steering vector. Since the actual signal is included in the covariance matrix estimate, small errors in the steering vector can cause a mismatch between the steering vector used in the algorithm and the true steering vector. This may cause the MVDR filter to underestimate the amplitude of the signal.

A common way to mitigate these problems is to add a positive *diagonal loading* term, $\alpha\mathbf{I}$, to the estimated covariance matrix $\widehat{\mathbf{R}}$. Diagonal loading corresponds to an assumption of additive white noise with variance α on the inputs. A high noise variance causes the beamformer to be "cautious", and thus, less adaptive; too low variance may lead to underestimation of the signal. Thus, there is a trade-off between adaptivity and robustness, and several approaches have been proposed to find an appropriate loading.

One approach is to make the loading proportional to the power of the received signal

$$\alpha = \frac{1}{\epsilon M} tr\{\widehat{\mathbf{R}}\}, \tag{3.25}$$

where ϵ inversely scales the amount of loading and $tr\{\}$ is the trace. This makes the loading proportional to the average power of the signals. Although this is reasonable since it adds less absolute loading if the signals are weak, ϵ is still a user parameter.

Different approaches to calculate an optimal loading term based on uncertainties in the steering vector have been proposed, for example by Li et al. in [43]. These approaches require the user to specify these uncertainties, which may be a challenging task. Li et al. further proposed approaches to automatically compute the level of diagonal loading in [44]. One such approach was successfully evaluated on ultrasound data by Du et al. [45].

3.10 Processing of broadband signals

The MVDR approach, along with many other advanced array processing methods, assume narrowband signals. The most straightforward way of handling broadband signals is to perform the processing on each separate frequency component in the frequency domain. This is done by replacing the narrowband covariance matrix by the *spectral matrix*, or *cross-spectral matrix*. The elements of the spectral matrix are the inter-element frequency wise correlations.

In (3.18) the sample covariance matrix was estimated by temporal averaging over a number of samples. The averaging reduces the variance of the estimated covariance matrix, and allows the estimated matrix to achieve full rank. Averaging is also necessary in the estimation of the spectral matrix. Since a sufficient number of samples are required for each frequency estimate used in the averaging, each block of the signal is segmented into N_f segments.

Performing a Fourier transform on each segment f from each element m, $g_{f,m}(t)$, results in $G_{f,m}(\omega)$. By forming

$$\mathbf{G}_f(\omega) = [G_{f,0}(\omega) \quad G_{f,1}(\omega) \quad \cdots \quad G_{f,M-1}(\omega)]^T, \tag{3.26}$$

the spectral matrix $\mathbf{G}(\omega)$ is estimated as

$$\widehat{\mathbf{S}}(\omega) = \frac{1}{N_f} \sum_{f=1}^{N_f} \mathbf{G}_f(\omega) \mathbf{G}_f^H(\omega), \tag{3.27}$$

The resulting set of spectral matrices can then be used for MVDR estimation, which is done in Paper I.

Since each frequency component is processed independently, this approach does not utilize the broadband nature of the signal and can therefore be considered as *incoherent*. Poor signal-to-noise ratio (SNR) or short data sets used for the FFT can lead to high variance in the estimates of the individual narrowband spectral matrices [46].

An alternate, *steered covariance matrix*, approach was proposed by Krolik [46]. By prealigning far-field signals to a particular direction, a steered covariance matrix can be formed as a parametrization in θ

$$\widehat{\mathbf{R}}_\theta = \frac{1}{N_s} \sum_{t=1}^{N_s} \mathbf{g}_\theta(t) \mathbf{g}_\theta^H(t) \tag{3.28}$$

where N_s is the number of samples, and

$$\mathbf{g}_\theta(t) = [g_0(t + \tau_0(\theta)) \quad g_1(t + \tau_1(\theta)) \quad \cdots \quad \cdots \quad g_{M-1}(t + \tau_{M-1}(\theta))]^T, \tag{3.29}$$

with $\tau_m(\theta)$ as the inter-element relative delays for signals impinging from angle θ. This prealignment is identical to the delay step in the DAS beamformer. As a consequence, the steering vector for all frequencies from the steered direction becomes equal to the unit steering vector, $\mathbf{1}^T$, enabling direct application of the MVDR solution in (3.19) on the steered covariance matrix. As a result the following weight vector is obtained

$$\mathbf{w} = \frac{\widehat{\mathbf{R}}_\theta^{-1} \mathbf{1}}{\mathbf{1}^H \widehat{\mathbf{R}}_\theta^{-1} \mathbf{1}}. \tag{3.30}$$

The resulting weight vector is then applied directly on the steered broadband signal $\mathbf{g}_\theta(t)$ as

$$y(t) = \mathbf{w}^H \mathbf{g}_\theta(t). \tag{3.31}$$

The MVDR estimation is thus performed on only one, broadband, covariance matrix. Note that the frequency components for interferers from other directions and wavenumbers are not aligned. Even a few broadband interferers may lead to a covariance matrix with high rank, which may in turn lead to poorer interference cancellation performance than would have been achieved by narrowband processing. However, short ultrasonic pulses result in a highly

non-stationary environment that requires the statistics to be estimated using only a short set of temporal samples. As discussed above, estimating spectral matrices under these conditions will lead to poor estimates. Some methods to increase the number of snapshots were discussed in Sec. 3.8.

The steered covariance matrix approach requires inversion of the covariance matrix for each angle, compared to the frequency domain approach where a single covariance matrix is estimated for each frequency. Since the formation of the steered covariance matrix also involves some processing, the steered covariance matrix approach tends to be more computationally demanding for most applications involving far-field signals.

3.A Phase-mode beamformers

In Section 3.4, the use of apodization, or windowing, for beampattern manipulation of standard beamformers was discussed. A significant amount of apodization design strategies for ULAs are available in the literature [33]. Unfortunately, these methods are not directly applicable to UCAs. However, transformation of the array steering vector into so called *beamspace* representation enables application of these methods on UCAs. Note that this is essentially a standard beamformer. More details on phase-mode beamforming can be found in Paper I, and a complete derivation of the approach is found in [33].

3.B Multiple signal classification

A completely different approach in array processing compared to the standard beamformer and MVDR, is the multiple signals classification (MUSIC) technique [47]. MUSIC is a so called subspace approach, which is based on the separation of eigenvector subspaces spanning the spatial covariance matrix. In common with the MVDR approach, MUSIC is not capable of handling correlated signals.

For direction of arrival (DOA) estimation of narrowband signals using a M element array, the first step of the method is to perform an eigenvalue decomposition of the $M \times M$ covariance matrix $\widehat{\mathbf{R}}$. Assuming that there are N_d impinging signals, the $M - N_d$ smallest eigenvalues will correspond to the eigenvectors of the covariance matrix spanning the noise subspace. The matrix $\widehat{\mathbf{N}}_e$ is formed using the noise subspace eigenvectors. The DOA's of the impinging signals are then found by searching for steering vectors $\mathbf{a}(\theta, k)$ corresponding to the N_d highest peaks of the function

$$\frac{1}{\mathbf{a}^H(\theta,k)\widehat{\mathbf{N}}_e\widehat{\mathbf{N}}_e^H\mathbf{a}(\theta,k)}. \tag{3.32}$$

MUSIC can also be used on broadband signals by repeating the procedure on each spectral matrix (3.27). However, this requires eigenvalue decompositions and estimation of the number of signals for each frequency band. An alternative method to was proposed in [48]. The approach is based on creating a broadband spectral matrix. This allows a single eigenvalue decomposition to be performed instead of one for each narrowband spectral matrix, which is very efficient if there are multiple signals with limited bandwidth in several different frequency bands. However, signals with wider bandwidth will be spanned by more than one eigenvector. Hence, the separation between the noise and signal subspace will break down and performance will be degraded.

4. Previous work on imaging using Lamb waves

The previous chapters covered the basics of Lamb wave theory and array processing which forms the foundation for array imaging of Lamb waves. This chapter reviews important work on this topic. The first section focuses on array imaging, which is most relevant for this thesis. The following sections concern some alternative approaches.

4.1 Array imaging

The use of array processing of Lamb waves for inspection of engineering structures is a fairly young field. Possibly the earliest work using a phased array on Lamb waves was reported by Deutsch et al. in 1997 [49] who proposed a method based on so called *time reversal* to focus a ULA on a defect. This is a somewhat unconventional case of array processing and it will be described separately in Section 4.2. In this section, work that is based on conventional array processing is covered.

A more general array approach was proposed by Wilcox et al. in [50]. Circular arrays with ceramic disc actuators, were proposed for omni-directional inspection of plate structures. Using a fully active array enabled acquisition of a dataset which was used for synthetic focusing.

In [51] Wilcox presented further developments of the concept and proposed a more sophisticated approach for processing data from omnidirectional guided wave arrays. The received data was dispersion compensated using the approach described in Section 2.A and a simulated array response was used in a deconvolution step to reduce the side lobes. Furthermore, experimental results using an EMAT array were presented and a subsequent publication [22] described in detail the design of an EMAT array. Following this line, Fromme et al. presented experimental results obtained using a compact, low power, active array employing piezoelectric transducer elements [52].

Giurgiutiu & Bao coined the name *embedded-ultrasonic structural radar* (EUSR)[53]. Their setup consisted of an active array of piezoelectric elements. Focusing was performed on both transmission and reception using a standard beamformer. They used an operating frequency range below the cut-off frequency for the A_1 mode, and a careful frequency selection improved the excitation of the S_0 mode while limiting the excitation of the A_0 mode.

Mode selectivity and a reduction of effects from dispersion was achieved by limiting the bandwidth of the excitation signal. Their later work included optimizing the size of the array elements to further improve pure excitation of the S_0 mode [23], and the evaluation of different array configurations [54].

Other work includes Moulin et al. [55], who experimentally evaluated the performance of beam steering on transmission on a composite plate using a three element linear array. Sundararaman et al. [56] examined different configurations of transmitter and receiver arrays in pitch-catch mode on both steel and composite plates. An adaptive approach based on least mean squares (LMS) was also considered, although no thorough evaluation of its performance was presented. Rajagopalan et al. [57] examined imaging using the conventional beamformer on weakly anisotropic multilayered composite plates. Dispersion compensation was performed using the approach in [51]. Yan and Rose [58] examined array beam steering in anisotropic plates.

Velichko and Wilcox evaluated different techniques to optimize the weight vector for a particular array configuration to achieve the highest resolution with the lowest possible sidelobes [59]. An extension of the approach for multiple modes was also presented. Note that their approach used a fixed weight vector, which reduces sidelobes even for angles where no interfering signals or modes exist, cf. end of Section 3.4. This should be contrasted to adaptive approaches that can potentially allow high sidelobes for angles where there are no interfering signals and instead focus on minimizing the contribution of actual interferers.

Recently, Yan et al. [60] experimentally evaluated a tomography setup and a circular array for imaging. The dispersion was compensated using the approach in [51]. Instead of performing synthetic focusing, as in for example [50], focusing was performed on transmission.

4.2 Time-reversal

Time-reversal is an autofocusing technique for waves. Probably the most common application of the time-reversal concept is for autofocusing of arrays. The principle is simple: All array elements are excited in phase with a broadband input signal. The signals are backscattered in the media and received by the array. By time-reversing the backscattered signals received by each element, the result will be an input signal that automatically focus on the strongest present scatterers [61].

The first use of a time-reversal concept for Lamb waves was probably by Alleyne et al. in [62]. A signal was transmitted into a plate and acquired with a receiver at some distance from the transmitter, after being subject to dispersion. By reversing and retransmitting the signal into the medium, the propagation restored the original signal, which improved the peak amplitude. Note that the work in [62], in contrast to Deutsch et al. [49], did not concern ar-

rays. Furthermore, the approach compensated dispersion for only a particular propagation distance.

Ing [63, 64] examined the time-reversal technique for focusing of arrays, where multiple modes and dispersion was automatically compensated for by the time-reversal. A disadvantage of the time-reversal approach is that it requires a significantly more advanced generator for the transmission than most other array processing techniques. Since a reversed signal waveform is used as an input signal, the generator is required to be fully programmable, a feature that is not available in standard ultrasonic instruments.

Deutsch et al. [49] used a simplified time reversal approach on a standard phased array. Instead of reversing the received signals, cross-correlation was used to determine time-of-flight of the back-scattered data from a single reflector. The time-of-flight estimates were used to apply proper delays on transmission and thereby focus on the defect. However, since no frequency-dependent phase information was determined, the dispersion could not be compensated for. It also utilized the fact that the A_1 mode had the highest group velocity in the frequency range, and could therefore be identified.

4.3 Tomography and distributed sensors

Compared to the array approaches reviewed above, tomography uses distributed sensors that surround the investigated area. The technique uses multiple projections to create an image of a region. The projections are created by insonifying the object from different positions and receiving the signals at the opposite side of the object. Early work focused on the so called parallel projection approach using, for example, immersion [65] or air-coupled transducers [66]. The parallel projection algorithm uses a transmitter-receiver pair of transducers that is mechanically moved in parallel over the region of interest and this cycle is repeated for a set of angles. Although good results can be achieved with this approach, the need of mechanical movement of the transducers requires a setup capable of accurate positioning of the transmitter and receiver in parallel, which complicates field inspections.

To avoid the need for mechanical movement of the setup, McKeon et al. [67] evaluated the crosshole technique, which borrows concepts from seismology. The crosshole approach does not rely on parallel transmit-receive paths. Instead the transmitted signal from each position is received at all receiver positions. This leads to a more efficient use of the setup, and is not restricted to a certain geometry which allows for fixed array setups. The technique is more suitable for field applications, such as SHM.

Compared to the approaches reported above that make no assumptions on the condition of the area before inspection, access to the defect free structure allows acquisition of baseline reference data. By subtracting the baseline reference signals from the current measurement data, the part of the signals orig-

inating from naturally occurring boundaries, e.g., edge reflections or welds are removed. The technique has been evaluated for imaging in SHM in several publications, for example, [68, 69, 70]. However, due to difficulties in repositioning of element positions and lack of reference data, this may not be suitable for temporary inspections.

If the baseline data is reliable, this allows high sensitivity to defects even with few sensors. However, baseline methods are sensitive to environmental changes, such as temperature, which may require multiple sets of reference data for different conditions. Some strategies to mitigate these issues were evaluated by Konstantinidis et al. in [69] and by Wilcox et al. in [71].

Michaels et al. [72] proposed the use of the MVDR algorithm on data from a tomographic setup. A multistatic dataset was acquired by sequentially exiting a number of transducers. The transducers encircled a single defect, which was probed by the transducers from different angles. This causes the backscattered signals from different excitations to vary substantially. To improve the results a scattering model of the defect was used to compensate for these variations. However, in the presence of multiple scatterers with complex scattering profiles, this may be a complicated approach.

A disadvantage with this type of methods is that cabling and positioning become more complex due to the distributed sensors. Furthermore, positioning of sensors close to edges may cause significant problems even due to small errors in the baseline data, since the edge reflections may overlap scattered signals from defects.

4.4 Synthetic aperture focusing techniques

The synthetic aperture focusing technique (SAFT) is a method that combines data acquired at different positions relative to the ROI and can be seen as a special case of general array processing. SAFT is usually performed using a single transducer in pulse-echo mode. The transducer is moved along a line and probes the region of interest at regular intervals, thereby illuminating each point in the region from different angles. Similar to DAS beamforming, the data from each transmission position is delayed and summed to coherently average the contributions from each point of interest, which reduces the interference from other scatterers.

The frequency dependent phase-velocity of Lamb waves requires a frequency dependent phase shift to achieve coherency for all frequency components. The use of SAFT on Lamb waves was proposed by Sicard et al. [73], and later evaluated for detecting corrosion defects in [74]. A mode selective excitation was required to avoid interference from other propagating Lamb modes, which was achieved using an angle beam transducer in the experimental results.

Note that SAFT requires numerous measurements with accurate positioning of the transducer to achieve high resolution images. Since mechanical positioning over large areas is generally difficult, this makes the method impractical in field inspections, and unusable for monitoring applications.

5. Array processing of Lamb waves

5.1 Introduction

Chapter 4 summarized some of the most significant work on Lamb wave imaging and it was indicated that previous work on array processing of Lamb waves, with few exceptions, has used standard beamformers of the type described in Section 3.2 and 3.3. These are robust, simple to implement and computationally efficient, but have poor performance compared to more advanced methods. One obvious way to improve the performance of the standard beamformer is to use a larger array. However, this might not be a feasible option due to space, hardware or economical limitations.

Advanced methods, such as adaptive beamformers, could potentially achieve much greater resolution and interference suppression. However, the lack of thoroughly analysed implementations of adaptive methods for Lamb waves raises the question if there are any particular issues related to Lamb waves limiting the applicability of more advanced array processing methods. This chapter summarizes the work presented in Papers I, II and III, on the development of an adaptive approach for Lamb wave imaging.

For many array processing applications, such as radar and medical ultrasound, the interference comes mainly from other reflectors than the target of interest, at distances making them overlap the relevant signal. These applications can be considered as single mode[1], since there are in most cases no waveguides present which could enable the existence of multiple modes. For Lamb waves, however, the interference may also come from other propagating Lamb modes travelling at different velocities. In addition to difficulties in identifying true defects from interfering modes, the dispersion of the Lamb waves reduces range resolution.

If mode selectivity could be effectively achieved, the dispersion could without difficulty be compensated, as described in Section 2.A. In Chapter 2 the use of mode selective transducers capable of exciting a single mode was discussed. However, these approaches require a signal with a relatively narrow bandwidth, resulting in a trade-off between bandwidth and mode selectivity.

[1]Modes as in waveguide modes, not to be confused with multipath propagation due to, for example, ground reflections in RADAR.

5.2 Wavenumber selectivity

Omni-directional coverage of an array setup is desirable to decrease the measurement time of inspections, and for efficient monitoring in SHM applications. As discussed in Chapter 3, a ULA is not a suitable array configuration for 360° coverage in general. For multimodal Lamb waves there is another implication worth noting: Lamb modes are propagating waves which may occupy the same frequency range, but travel at different phase-velocities, and thus, different wavenumbers.

To illutrate the problem, consider a ULA with two signals impinging from 0° as illustrated in Figure 5.1. The impinging signals have different wavenumbers, but since the steering vector of the ULA (3.5) at 0° is independent of wavenumber and is simply the unit vector $\mathbf{1}$, both signals satisfy the steering vector. Thus, while the angular resolution is highest at 0°, the wavenumber resolution is poorest. At 90° the opposite situation occurs, angular resolution is poor and wavenumber resolution is high. A 2D array, on the other hand, is not only capable of omni-directional angle resolution, but also omni-directional wavenumber resolution. The drawback is that many array elements are required to achieve sufficient resolution for all angles and wavenumbers.

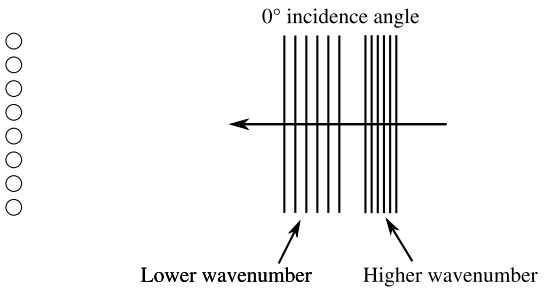

Figure 5.1: Two plane waves with different wavenumbers impinging from 0° angle at an eight element ULA.

In summary, the combination of 2D arrays and advanced array processing methods can potentially improve imaging resolution and more efficiently suppress interference from other scatterers and interfering Lamb modes compared to standard beamforming. The best performing methods in array processing are parametric, derived using, for example, a maximum likelihood approach [75]. However, for these methods to be computationally tractable, an accurate signal model is required, which may be difficult to obtain [76]. Recall from Section 2.6 that Lamb waves both change in shape and may convert to other modes at reflection. In addition, a signal model for each separate Lamb mode is also required to allow for mode dependent reflection coefficients. Formulating such a model may lead to an undesirable high number of degrees of freedom. Hence, such methods might not be feasible in practical

applications. This motivates an evaluation of methods that do not require such a detailed signal model.

By considering a basic problem, such as, direction of arrival estimation of a passive source, insight could be gained into properties of Lamb waves that might affect the applicability of different methods on the Lamb wave imaging problem.

5.3 Paper I - Direction of arrival estimation

Paper I provides an evaluation of three methods that do not require knowledge about the signal waveform, a phase-mode beamformer (PMBF) approach, the MVDR (or Capon) method, and the multiple signal classification (MUSIC) technique. The purpose of the evaluation was to give insight into the properties of Lamb waves that might affect the applicability of the MVDR and MUSIC approaches, as well as other methods. The methods were evaluated on both simulated and experimental data.

The setup modelled a passive acoustic emission scenario, where an active transducer emits a multi-cycle sinusoid that propagates in a plate and is received by a passive UCA. It was assumed that the dispersion characteristics of the plate were unknown, as well as the number of propagating modes, making the problem a general frequency-wavenumber estimation problem. For each frequency, the power of each angle/wavenumber ($\theta - k$) pair was to be estimated. The angular power spectrum was then estimated by summation over all wavenumbers for each angle.

In Sections 3.8 and 3.B, the MVDR and MUSIC methods inability of handling correlated signals was discussed. In the work presented in Paper I it was assumed that the impinging signals were uncorrelated, thereby avoiding the need of preprocessing, such as spatial smoothing, cf. Section 3.8.

The results showed that the MVDR approach and, to some extent, the MUSIC approach performed significantly better on both simulated and experimental data, in terms of higher resolution and lower sidelobes than the phase-mode beamformer, which is basically a standard beamformer. It was further shown that the MVDR beamformer and the MUSIC approach was less sensitive to the "false" grating lobes in the UCA's array pattern discussed in Section 3.7. This could allow a less dense, and possibly irregular, array which would improve resolution without increasing the number of elements in the array. This is particularly useful in the presence of multiple modes, since the modes may span a large range of wavenumbers. However, the most significant drawback of the MVDR and MUSIC approaches when considering imaging are their inability to cope with correlated signal.

5.4 Lamb wave imaging

The findings encouraged further investigations on extending the methods from the passive array case to an active setup as this would enable imaging. This is the topic of Papers II and III.

The objective of the plate imaging problem is obviously an accurate representation of defects in the plate. It can be assumed that the plate is finite and that the defects have arbitrary shape and are likely to appear at any part of the plate. Thus, both near- and far-field coverage using a two dimensional array is essential. It is also desirable that the proposed method works with both single and multiple transmitter setups. Furthermore, broadband signals are required for high range resolution, and finally, the backscattered signals can be assumed to be highly correlated.

5.4.1 Model

To provide some insight for the reader into the properties of the setup that are relevant for imaging, a simplified model is used. Assume that there are R point-scatterers in the plate that scatter incident waves equally in all directions and that no multiple scattering occur between scatterers. Further assume that the array elements are point-like and perfectly omni-directional in both transmission and reception. Hence, assuming also that the output from each element is equal to the normal surface displacement, the output from receiving element m, $G_m(\omega)$, is the sum of the contributions from all possible mode combinations for all scatterers r for transmitter p as

$$G_{p,m}(\omega) = \sum_{r=1}^{R} \sum_{n,n'} \frac{1}{\sqrt{z_{r,p} z_{r,m}}} R_{r,n,n'}(\omega) \cdot H_n(\omega) \mathcal{T}(\omega) e^{j(k_n(\omega)\|\mathbf{z}_r - \mathbf{z}_m\| + k_{n'}(\omega)\|\mathbf{z}_r - \mathbf{z}_p\|)} \quad (5.1)$$

where $z_{r,p} = \|\mathbf{z}_r - \mathbf{z}_p\|$ and $z_{r,m} = \|\mathbf{z}_r - \mathbf{z}_m\|$; $\mathbf{z}_r$, $\mathbf{z}_m$ and $\mathbf{z}_p$ are the positions of the scatterer, the receiving element, and the transmitting element, respectively. The transfer function $H_n(\omega)$ describes the coupling between an exciting stress $\mathcal{T}(\omega)$ and the resulting normal displacement of mode n. The point scatterers are assumed to have an unknown, frequency and mode dependent reflection coefficient $R_{r,n,n'}(\omega)$, where n is the incident mode and n' the reflected mode. In the case of mode conversion, n and n' will differ.

5.4.2 Paper II – Single transmitter imaging

Paper II concerns the use of a single transmitter – multiple receiver setup for performing imaging of a plate.

In Secion 3.10 the steered covariance matrix (STCM) was described as an alternative approach to frequency domain processing. A modification of the

STCM approach has been used to perform focusing in near-field medical ultrasound imaging in [42, 40, 41]. This approach results in a broadband covariance matrix focused both in angle and range, thereby requiring one covariance matrix inversion for each point. However, for broadband dispersive Lamb waves, simply using delays will not align the signals since the frequency components propagate at different phase velocities. A solution to this problem was proposed in Paper II. By combining the steering operation with dispersion compensation, cf. Sec 2.A, a focused covariance matrix was estimated for a potential scatterer in each point.

Several snapshots are required for covariance matrix estimation. As discussed in Sec 3.10, averaging over adjacent points may not be a feasible approach for broadband signals. In addition, such averaging does not decorrelate the signals. Since only one transmitter were available spatial smoothing was employed. However, as discussed in Sec. 3.8, spatial smoothing requires a regular array shape to form identical subarrays. Hence, in Paper II a URA was used, which is a suitable selection allowing 360° coverage.

An evaluation of the method was performed on both simulated and experimental data. For the experimental evaluation a number of defects were added to the aluminium plate used for the results in Paper I. The defects were pairs of drilled through holes, a 1 cm wide notch, and some artificial pits with depths of 1 to 3 mm as seen in Figure 5.2. A simplified model of the plate was used for the simulation results.

Figure 5.3 shows results from simulated data and Figure 5.4 from experimental data. Both the simulated and experimental data show that the MVDR approach yields much higher resolution and interference suppression than the standard beamformer. It was further shown in the paper that the proposed method performs better in terms of interfering Lamb mode suppression.

Issues related to uncertainties in the array steering vector and correlated signals were discussed. These typically result in underestimation of amplitudes, which could be seen in some of the results.

5.4.3 Paper III - Multiple transmitter imaging

A natural extension of the method presented in Paper II, was to use multi-transmitter data. By creating a full multistatic set using all array elements as both transmitters and receivers, issues related to correlation between sources are eliminated. Furthermore, since spatial smoothing is avoided, much smaller arrays could be considered. Simulated and experimental data was used to compare the performance of the MVDR approach and the standard beamformer.

Simulations were performed on different array geometries and sizes. A single reflection of the S_0 and A_0 modes was simulated and the algorithms ability to focus on one mode and suppress the other using various array configurations was evaluated. The performance of the methods was also evaluated in the presence of mode conversion.

The paper also discusses issues related to focusing of broadband signals when using multiple transmitters. It was shown how the different transmitter-receiver pairs creates elliptic shaped focus lines which may cause a single scatterer to appear spatially smeared between the transmitter snapshots. Furthermore, different defects may appear in different snapshots, which increases the number of interferers in the estimated covariance matrix. This reduces the efficiency of MVDR beamformer. A method to mitigate these effects is proposed and discussed.

Examples of results presented in the paper can be seen in Figure 5.5 for simulated data and Figure 5.6 for measured data. Again, the MVDR approach clearly outperforms the standard beamformer. In the paper, comparisons of the performance for different array sizes and configurations show that the MVDR approach can allow smaller arrays without reduced performance compared to a standard beamformer on a larger array. It was further shown using simulated data that 2D arrays in conjunction with the proposed approach yields much more efficient suppression of interfering Lamb modes compared to the standard beamformer.

5.5 Conclusions

It has been shown that a two dimensional array in conjunction with a MVDR beamformer can significantly improve resolution and interference suppression in plate imaging. Due to the MVDR approach's inability to handle correlated sources, a decorrelating preprocessing step is required for single transmitter setups which reduces the effective aperture size. By contrast, multiple transmitter setups do not have this limitation, thereby allowing full aperture utilization.

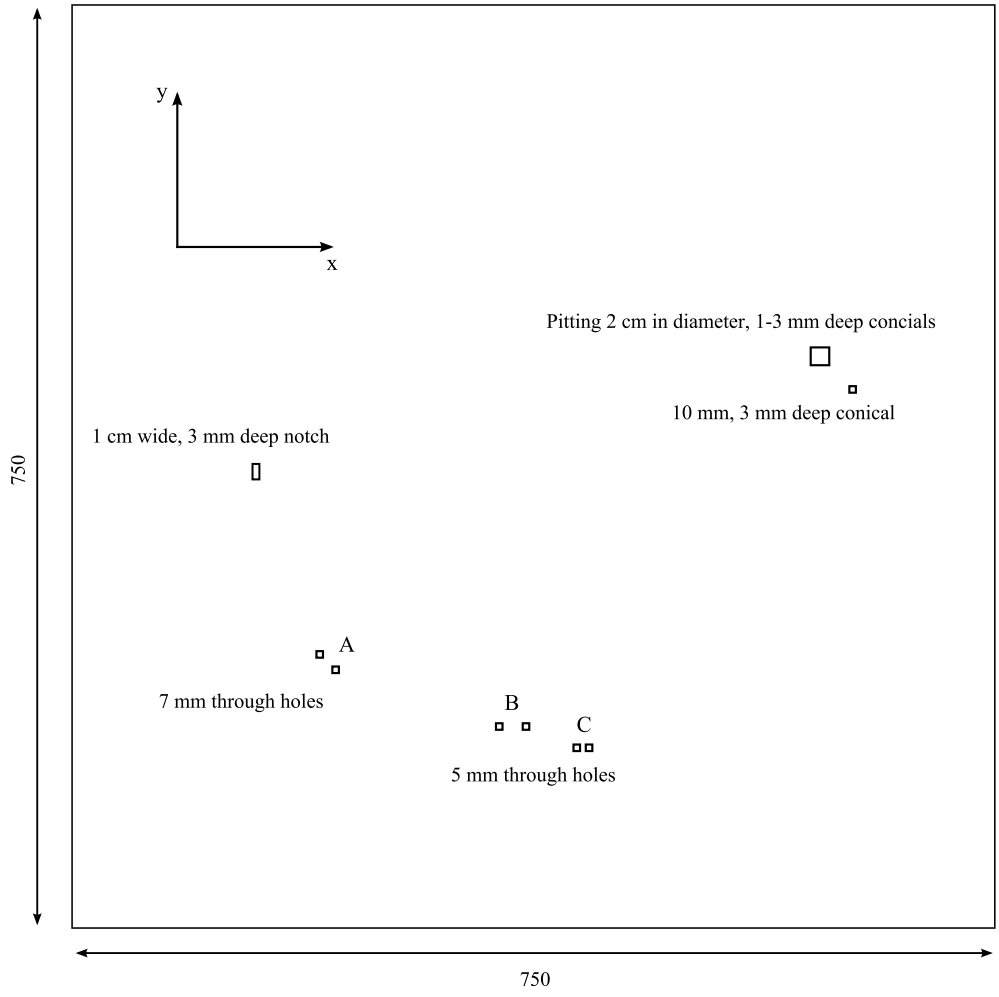

Figure 5.2: Layout of the aluminum plate with artificial defects. In the results, the arrays were positioned in the center of the plate.

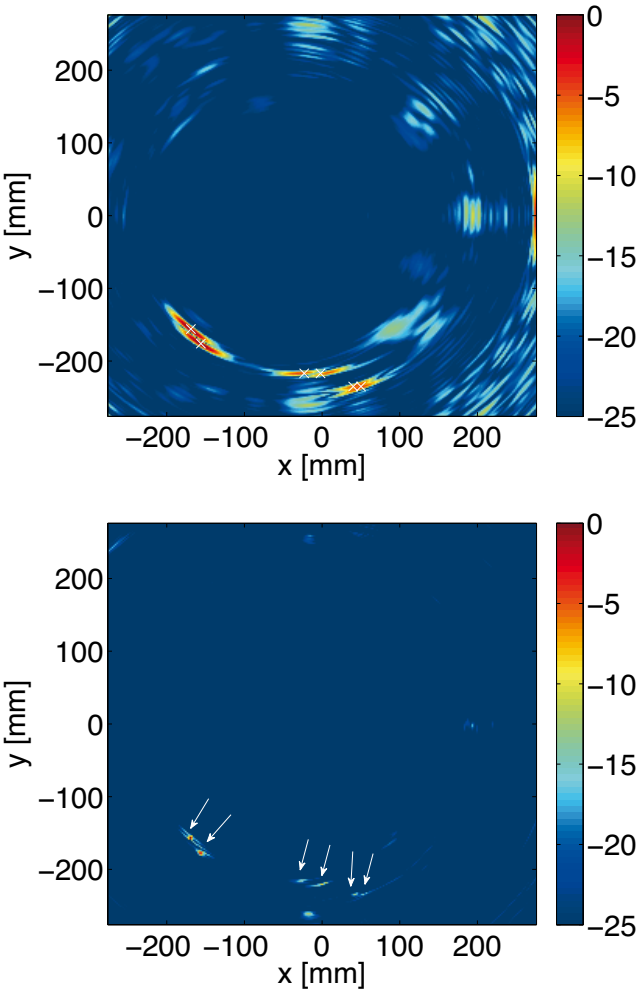

Figure 5.3: Results from simulated single transmitter data using standard beamformer (top) and MVDR approach (bottom). White crosses or arrows show which peaks that are actual defects. The resolution of the MVDR approach is significantly higher. The interference shown in the top plot, which is mainly due to interfering modes, is mostly supressed by the MVDR approach.

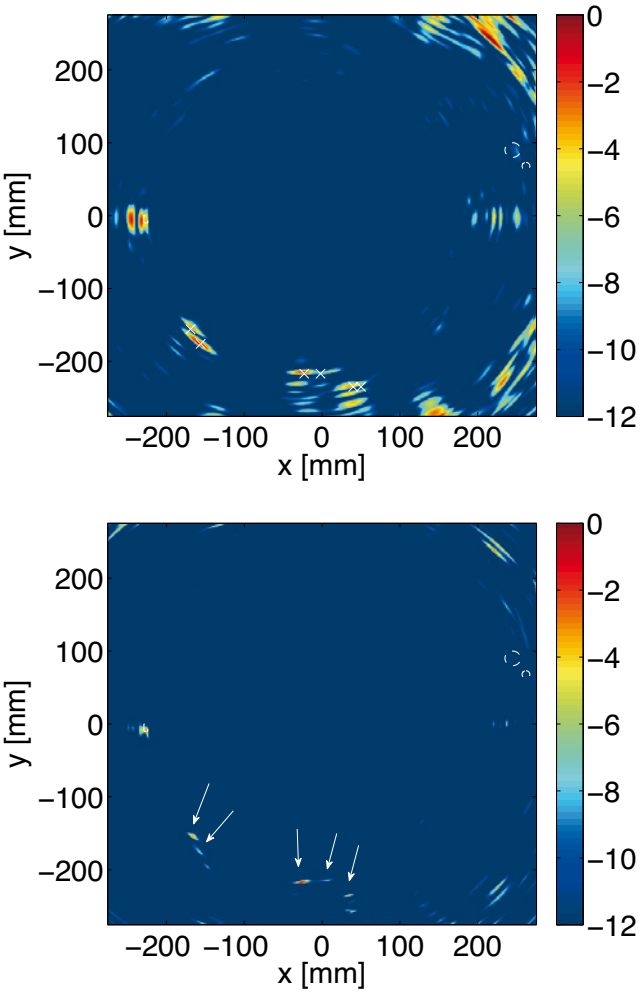

Figure 5.4: Results from experimental single transmitter data using standard beamformer (top) and MVDR (bottom). White crosses or arrows show which peaks that are actual holes. The dashed lines show the positions of the pits and the notch, in the center right and center left, respectively. Resolution and interference suppression is significantly better with the MVDR approach.

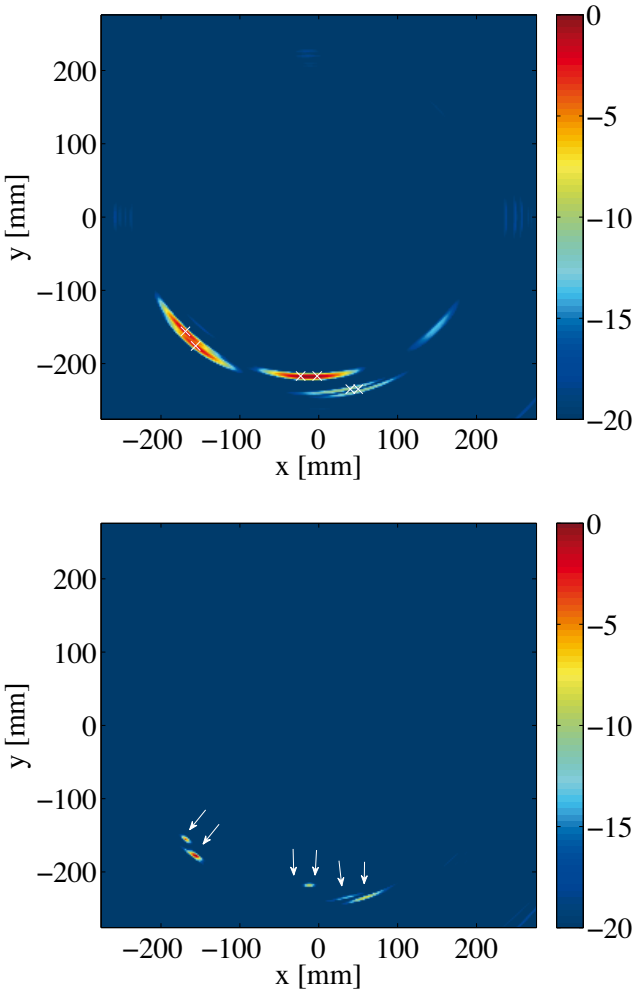

Figure 5.5: Results from simulated multi-transmitter data using standard beamformer (top) and MVDR (bottom). White crosses or arrows show which peaks that are actual defects. Resolution and interference suppression is significantly better with the MVDR approach. The center holes (pair B, cf. 5.2) are not resolved by either of the methods.

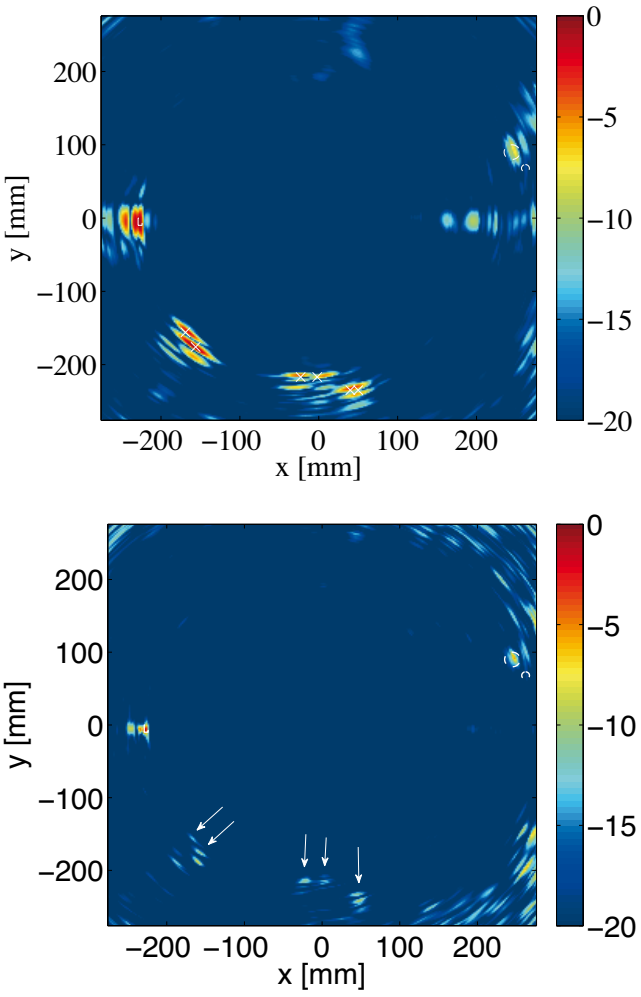

Figure 5.6: Results from experimental multi-transmitter (3×3 transmitter array) data using standard beamformer (top) and MVDR (bottom). White crosses or arrows show which peaks that are actual holes. The dashed lines show the positions of the pits and the notch, in the center right and center left, respectively. Resolution and interference suppression is significantly better with the MVDR approach. However, the amplitudes of the holes were underestimated.

6. Resonance based methods for the inspection of plate structures

6.1 Introduction

The previous chapters in this thesis concerned the use of propagating Lamb waves for the inspection and monitoring of structures. That can be regarded as a time domain approach, since range resolution is achieved through temporal separation.

This chapter concerns the use of resonance techniques for inspection, which is the topic of Papers IV, V and VI. The work was funded by two EU projects, INCA and NANOSCAN. The participation in these projects involved the development and evaluation of ultrasonic resonance methods to inspect carbon fiber reinforced plastic (CFRP) panels, and multilayered structures used in aerospace applications. Within the INCA project, special attention was given to *weakened bonds*. As the name implies, a weakened bond is an adhesive bond where there is contact between the interfaces, but its strength is decreased. Since the elastic properties of the interface changes very little, this type of defect is very difficult to detect. By contrast, a complete disbond creates a significant change in the interface and is in many cases detected without difficulty.

An extensive amount of research has focused on the development and evaluation of ultrasonic techniques for NDT of adhesive joints. In Chapter 1, Lamb waves were mentioned as one possible technique [5, 6, 7]. Another approach is mechanical impedance analysis (MIA) which has some similarities to the resonance techniques discussed below [77, 78]. Adams and Cawley [79] reviews NDT techniques and defect types that can occur in bonded joints and composites.

An object's natural modes of vibration are a valuable source of information on the condition of the material. Some approaches, such as resonant ultrasound spectroscopy (RUS) [80], use techniques to directly measure the resonance frequencies of the object. For objects with simple geometries these resonance frequency measurements, in conjunction with a physical forward model of the object, enable estimation of the object's material properties. However, complex objects are not suitable for this type of estimation due to the difficulty involved in creating an accurate model. Hence, a more production oriented application of this method has been developed based on the detection of changes

in the spectrum, so called *resonance inspection*. Using a large set of good and bad units as training data, units are either passed or failed during the test.

Another approach to utilize an object's resonance frequencies for testing, is to place on the inspected object a resonant transducer that is acoustically coupled through a thin layer of couplant. A frequency sweep over a limited band is performed and an application tailored instrument measures the electrical impedance of the probe for a range of frequencies. This means that it is not the resonance spectrum of the structure that is observed, but the resonance spectrum of the transducer coupled to the structure. The mechanical load the structure exerts on the transducer will alter the frequency response of the transducer. Changes in the position of the resonance frequencies are then used to detect defects. Since only a limited volume of the inspected object, in the close vicinity of the transducer, is excited, these inspections are local. The technique is available in some commercial instruments, such as the Fokker Bond-Tester.

6.2 Narrowband Ultrasonic Spectroscopy

Instead of estimating the properties of certain resonances, such as frequency or peak-width, the complex valued electrical impedance of a transducer can be measured at a single frequency. This approach will be referred to as Narrowband Ultrasonic Spectroscopy (NBUS) throughout this thesis, to contrast it to the previously described method used in the Fokker Bond-Tester. As for that method, the transducer is acoustically coupled to the inspected object through a thin layer of couplant, for example, water or oil, as illustrated in Figure 6.1. Defects within the object will result in a change of the load sensed by the transducer, which can be detected as a change in electrical impedance.

Typically the operator monitors the measurements by observing the impedance change in the impedance plane between different samples or locations on the object. These measurements are therefore relative, which means that the impedance measured at the inspected area is compared to the impedance corresponding to a reference area, preferable defect free. The technique resembles eddy current inspection but a piezoelectric transducer is used instead of a coil.

This technique has been implemented in some commercial instruments, for example the BondMaster[1] series and BondaScope 3100[2]. Setting up an inspection for impedance measurement involves selecting a transducer and a working frequency, which is usually set automatically to the resonance frequency of the transducer. The most common application of the approach is

[1] Olymbus NDT
[2] NDT Systems, Inc.

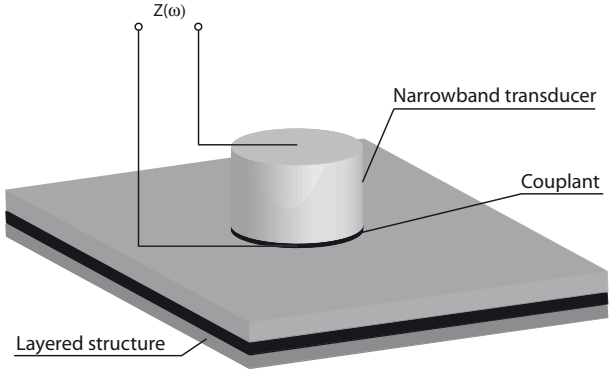

Figure 6.1: General NBUS setup (transducer housing and connector are omitted for clarity).

for detecting disbonding in multilayered structures. A disbond is a condition where the adherents are no longer bonded.

6.3 Paper IV – Experimental evaluation

In Paper IV, a model of a narrowband ultrasonic spectroscopy setup is presented along with experimental results from the measurements on aluminium-epoxy structures and CRFPs.

In order to evaluate the basic potential and limitations of the technique, measurements where performed on different defects using various transducers and working frequencies. Experimental results from measurements on simulated delaminations in aluminium-epoxy structures and CRFPs showed that transducer and frequency selection are not crucial in those cases. This was not surprising since a delamination completely changes the mechanical impedance of the object. However, the amplitude of the impedance change varied significantly between different transducers and frequencies. Detection of weakened bonds, on the other hand, proved to be very difficult, and a wide range of transducers and resonance frequencies were tested. This encouraged development of a model which could be used to provide insights and predict the performance of different setups.

6.4 Paper V & VI – Transducer design

Paper V and VI concern transducer design and the identification of relevant properties of transducers and suitable working frequencies. The basis for the work was a suitable simulation model.

The simulations were performed using simplified models of the transducer coupled to the layered structure. These models were based on a one dimensional approximation, that is, both the transducer and the structure were assumed to be laterally infinite resulting in only thickness motion. A large plate structure can with good accuracy be regarded as semi-infinite. However, this can not be assumed in general for a transducer. Therefore, parallel to the one-dimensional model a finite element model was used as a reference, where the effects of the lateral boundaries of the transducer were taken into account.

The sensitivity, that is, the amplitude of the impedance shift for different transducers and frequencies was simulated with respect to two parameters, couplant thickness and the presence of defects. There is no universal model for weakened bonds since the weakness can be caused by a number of problems, such as, contamination between the adherent and the adhesive, and porosity in the adhesive. The comparison was therefore made by modeling a thin interface layer between the adhesive and the adherend. Initially this layer had the same properties as the adhesive, but by introducing a small change in its elasticity, the resulting change in impedance of the transducers could be compared. This is covered in Paper V.

Paper VI offers an interpretation of the simulation results. Two factors were identified that fundamentally determine the performance of the measurement: the standing wave pattern formed in the structure, and the efficiency of the conversion between mechanical and electromechanical energy, the so called, effective electro-mechanical coupling coefficient (EMCC). When the standing wave in the transducer coupled to the structure, matches that of the free resonating transducer, the sensitivity is maximized. These factors depend on the working frequency and the transducer design. Transducer design essentially involves proper selection of the geometry of the piezoelectric element, which determines the resonance frequency of the transducer.

6.5 Conclusions

The performance of narrowband ultrasonic spectroscopy inspections highly depends on the transducer type and the selected working frequency. Defects, such as disbonds, are readily detected without careful tuning of the setup. However, weakened bonds are much more difficult to detect. Optimal transducer design and working frequency selection may increase the sensitivity of the inspection to certain defects.

7. Conclusions

The abundant use of plates in engineered structures and vehicles has stimulated the development of techniques for NDT and SHM. The first part of this thesis considers the use of arrays for Lamb wave inspection and monitoring of plates. Since Lamb waves can propagate over large distances, a large area of a plate can be covered by a single array.

The results presented in this thesis show that two-dimensional (2D) arrays enable not only angular selectivity, but also wavenumber selectivity. Wavenumber selectivity enables reduction of the interference from other Lamb modes. A review of previous research indicated that most of the presented work, with few exceptions, were based on standard beamforming methods. However, for a 2D array setup to have sufficient resolution in all directions for all wavenumbers, while maintaining low sidelobes, standard beamforming methods may require a large number of elements, which may be prohibitive due to practical and economical reasons.

A novel approach for plate imaging using Lamb waves was presented. Extending the use of the MVDR approach, which has previously been applied in other fields of array imaging, to handle dispersive and multi-modal waves resulted in a significant improvement in terms of resolution and suppression of interference from nearby defects and interfering Lamb modes. Efficient suppression of interfering modes allows wider bandwidth of the probing pulses, which improves range resolution and allows more flexibility in the array element design.

The main drawback of the method, its inability to resolve correlated sources, can be mitigated either through spatial smoothing, for single transmitter data, or through the use of multiple transmitters. However, spatial smoothing reduces the effective aperture size which is a disadvantage for single transmitter setups. The use of multiple transmitters eliminates this issue, thereby enabling full aperture utilization. Hence, multiple transmitter setups are preferred.

A comparison between the MUSIC, MVDR and a standard beamformer approach on a UCA showed that the MVDR and MUSIC approaches are less sensitive to, so called, false grating lobes. This enables the use of irregular arrays, which may be not be usable for standard beamformers due to grating lobes.

The second part of the thesis concerns resonant ultrasound inspection techniques of primarily multi-layered plate structures. Simulations and theoretical

argumentation showed that the working frequency and the transducer's resonance frequency, which is determined by the type and geometry of its piezoelectric element, greatly affects the attainable sensitivity. Optimal conditions occur when the standing wave pattern formed in the transducer and the structure, matches that of the free resonating transducer. This leads to the highest efficiency in the conversion between electrical and elastic energy, which ultimately leads to the highest sensitivity.

8. Future Work

There are several interesting future directions to explore. A few will be briefly mentioned below.

In this thesis the experimental evaluation of the adaptive imaging approach was performed on isotropic homogeneous materials only. However, if dispersion characteristics are available, the method can also be applied to anisotropic or multi-layered plates. Such experimental investigations would be of interest on for example composite structures.

In the presented results, no previous data is reused in the algorithm. This may be reasonable when performing a regular inspection. However, for SHM applications, measurement data may be available from before the actual damage occurred. Including such baseline data into the method could improve robustness and sensitivity.

Other signal processing approaches could also be considered. For example, the iterative adaptive approach (IAA) is a nonparametric weighted least squares based method which has been applied to a wide range of problems [81, 82, 83, 84]. Initial results have shown that there are several potential Lamb wave applications which would benefit from the approach, such as decomposition of Lamb modes, frequency-wavenumber estimation and beamforming. In contrast with the MVDR approach, the IAA method works in both coherent environments and can perform well even with only a few snapshots.

An evaluation of model-based approaches would be highly interesting, since such methods typically outperform other methods in scenarios where accurate prior information is available. However, the number of unknowns may be significant, leading to models with a large number of degrees of freedom. Furthermore, the complicated response of the transducer–plate coupling for different modes may require a complicated calibration procedure. Although such approach would be of academic interest, its impact in the field are likely limited.

9. Swedish Summary

9.1 Oförstörande provning

Plåtstrukturer är vanligt förekommande i världen omkring oss. Flygplan, båtar och cisterner är bara några exempel på fordon eller konstruktioner bestående av en betydande del platta eller svagt krökta plåtar. Många av dessa tillämpningar har höga säkerhetskrav vilket kräver kontinuerlig inspektion. I många fall kan en okulär besiktning vara tillräcklig, men för kritiska delar av en konstruktion kan det krävas mer sofistikerade metoder för att bestämma materialets inre tillstånd. I de flesta fall finns krav på objektets fortsatta funktionalitet vilket sammanfattar begreppet oförstörande provning (OFP).

Oförstörande provning är inte *en* teknik, utan ett samlingsnamn för en mängd olika tekniker baserade på olika fysikaliska principer till exempel, magnetism, röntgen eller värmeledning. En teknik som haft stor betydelse för en mängd olika tillämpningar är användandet av högfrekventa elastiska vågor, eller ultraljud. Ultraljudet genereras och tas emot av en sensor kopplad till ett instrument. En vanlig mätprincip, vilken även används för medicinska tillämpningar, är så kallad pulsekomätning. En kort puls genereras som propagerar in i materialet och eventuella förändringar i materialets egenskaper, naturliga eller skador, resulterar i att en del av pulsen reflekteras. Genom att samla in dessa ekon och söka efter avvikelser, kan man dra slutsatser angående materialets tillstånd. Efterbehandlingen är en viktig del av undersökningen där sofistikerade signalbehandlingsmetoder kan användas för att ta fram användbar information ur en signal som vid första anblick kan se helt slumpmässig ut.

De senaste tjugo åren har en ansenlig mängd forskning fokuserat på vad många anser vara nästa stora steg inom området – structural health monitoring (SHM)[1]. Idén bygger på att sensorer integreras i en konstruktion som därmed kan övervakas kontinuerligt. Genom att tidigt varna för problem kan säkerheten förbättras och kostnader förenade med större haverier minskas.

Denna avhandling behandlar två olika tekniker för inspektion av plåtar. Den första delen handlar om propagerande elastiska plåtvågor och den andra om så kallad resonansprovning.

[1] I brist på vedertaget svenskt begrepp.

9.2 Lamb vågor

När ett materials storlek i en eller två riktningar närmar sig våglängden för elastiska vågor i materialet, börjar det bete sig som en vågledare. Vågledare leder den propagerande vågen, vilken under rätt omständigheter kan färdas långa sträckor utan betydande dämpning. En typ av dessa vågor som uppkommer i tunna plåtar är så kallade Lamb vågor. Den långa räckvidden för dessa vågor möjliggör undersökning av en större yta av materialet från en fix position. De senaste årens forskning har lett till ökad förståelse om hur dessa vågor beter sig när de propagerar i olika material och i synnerhet hur de reflekteras. Svårigheten med dessa vågor är att de kan propagera i flera olika moder. Detta innebär att en enda puls som skickas in i plåten kan dela upp sig i flertalet så kallade moder som färdas med olika hastigheter. Dessutom är dessa vågor dispersiva, vilket innebär att pulsen kommer att smetas ut allt eftersom den färdas. Dessa två egenskaper gör analysen av dessa vågor mycket komplicerad.

Flertalet publikationer de senaste tio åren har behandlat användandet av grupper av sensorer, så kallade arrayer. Dessa placeras ut på en mindre yta av plåten. Sensorerna genererar en Lambvåg som sprider sig i plåten. På samma sätt som den ovan beskrivna pulsekotekniken, kommer avvikelser i plåten att resultera i att en del av vågen reflekteras. Dessa reflektioner tas emot av arrayens sensorer och kan sedan analyseras i en dator för att rekonstruera en avbildning av plåtens avvikelser. Exempel på sådana avbildningar visas i figurerna 5.3–5.6. Tänkbara tillämpningar för dessa arrayer är både tillfälliga inspektioner och SHM. I SHM kan ett antal sådana arrayer övervaka en större del av en plåt.

Den första delen av denna avhandling beskriver utvecklingen av en signalbehandlingsmetod för att rekonstruera dessa avbildningar. Tidigare publikationer inom området har varit begränsade till metoder som inte tillvaratar informationen i de insamlade signalerna på ett effektivt sätt. Den föreslagna metoden kan på ett mer sofistikerat sätt filtrera bort störningar som uppkommer av att flera moder propagerar i plåten. Dessutom ger metoden betydligt högre upplösning än vad som åstadkommits tidigare.

9.3 Resonansprovning

Den andra delen av denna avhandling berör så kallad resonansprovning. Genom att mäta plåtens så kallade självsvänging, eller resonans, fås betydande information om tillståndet inuti plåten. Dessa tekniker har främst använts för provning av flerlagerstrukturer och kompositmaterial. Metoderna fungerar så att en sensor placeras på materialet som ska undersökas. Sensorn är kopplad till ett instrument som får sensorn att vibrera med hjälp av en växelspänning. Genom att sensorn har kontakt med materialet, kommer en

del av den mekaniska rörelsen hos sensorn att fortplanta sig ner i materialet och reflekteras mot dess undersida. För vissa frekvenser hos växelspänningen kommer resonans att uppstå i både sensorn och materialet tillsammans. Vid förändringar i materialet kommer dessa frekvenser att påverkas. En vanlig typ av fel denna metod kan upptäcka är så kallad delamingering. Delaminering innebär att fogen som håller ihop två lager i en flerlagerstruktur inte längre håller ihop materialen. Denna del av avhandlingen beskriver genom simuleringar och teoretiska resonemang vilka egenskaper dessa sensorer bör ha för att maximera känsligheten för olika typer av defekter.

10. Acknowledgements

Jag vill börja med att tacka min handledare Tadeusz Stepinski för att jag fått möjligheten att utföra detta arbete och som under hela denna tid varit väldigt engagerad i arbetet, vilket har varit ovärderligt.

Ett särskilt stort tack till Tomas Olofsson som ägnat mycket tid till att läsa avhandlingen och manuskripten samt kommit med tydliga förslag till förbättringar.

Tack också alla nuvarande och tidigare kollegor på Signaler och system. Det har varit kul att tillbringa denna tid tillsammans med er. Tack för alla intressanta diskussioner.

Jag vill också tacka alla mina vänner utanför jobbet. Hoppas att vi får mer tid tillsammans efter det här, trots barn och allt! Särskilt vill jag tacka mina kompisar i bandet. Våra rep och inspelningar har varit viktiga avbrott.

Ett stort tack också till mina svärföräldrar Ove och Anita. Jag är tacksam för att ni ställt upp för oss!

Tack mamma, pappa och Sandra för att ni alltid finns där!

Sist men inte minst vill jag tacka min familj, Annelie, Elias och Filip. Ni är det bästa och viktigaste som finns! Jag är så glad att jag har er!

Bibliography

[1] C. R. Farrar and K. Worden. An introduction to structural health monitoring. *Philosophical Transactions of the Royal Society A: Mathematical, Physical and Engineering Sciences*, 365(1851):303–315, 2007.

[2] P. Cawley, M. J. S. Lowe, D. N. Alleyne, B. Pavlakovic, and P. D. Wilcox. Practical long range guided wave testing: Applications to pipes and rail. *Materials Evaluation*, 61(1):66–74, 2003.

[3] J. L. Rose. A baseline and vision of ultrasonic guided wave inspection potential. *Journal of Pressure Vessel Technology*, 124(3):273–282, 2002.

[4] D. C. Worlton. Experimental confirmation of Lamb waves at megacycle frequencies. *Journal of Applied Physics*, 32(6):967–971, 1961.

[5] S. I. Rokhlin. Lamb wave interaction with lap-shear adhesive joints: Theory and experiment. *The Journal of the Acoustical Society of America*, 89(6):2758–2765, 1991.

[6] M. J. S. Lowe and P. Cawley. The applicability of plate wave techniques for the inspection of adhesive and diffusion bonded joints. *Journal of Nondestructive Evaluation*, 13(4):185–200, 1994.

[7] J. L. Rose, K. M. Rajana, and M. K. T. Hansch. Ultrasonic guided waves for NDE of adhesively bonded structures. *The Journal of Adhesion*, 50(1):71–82, 1995.

[8] E. Lehfeldt and P. Höller. Lamb waves and lamination detection. *Ultrasonics*, 5(4):255–257, 1967.

[9] T. L. Mansfield. Lamb wave inspection of aluminum sheet. *Materials Evaluation*, 33(4):96–100, 1975.

[10] D. N. Alleyne and P. Cawley. Optimization of Lamb wave inspection techniques. *NDT & E International*, 25(1):11–22, 1992.

[11] D. E. Chimenti and R. W. Martin. Nondestructive evaluation of composite laminates by leaky Lamb waves. *Ultrasonics*, 29(1):13–21, 1991.

[12] N. Guo and P. Cawley. The interaction of Lamb waves with delaminations in composite laminates. *The Journal of the Acoustical Society of America*, 94(4):2240–2246, 1993.

[13] Z. Su, L. Ye, and Y. Lu. Guided Lamb waves for identification of damage in composite structures: a review. *Journal of sound and vibration*, 295(3-5):753–780, 2006.

[14] A. Raghavan and C. E. S. Cesnik. Review of guided-wave structural health monitoring. *Shock and Vibration Digest*, 39(2):91 – 114, 2007.

[15] J. L. Rose. *Ultrasonic Waves in Solid Media*. Cambridge University Press, 1999.

[16] J. D. Achenbach and Y. Xu. Wave motion in an isotropic elastic layer generated by a time-harmonic point load of arbitrary direction. *The Journal of the Acoustical Society of America*, 106(1):83–90, 1999.

[17] I. I. Nunez, R. K. Ing, C. Negreira, and M. Fink. Transfer and Green functions based on modal analysis for lamb waves generation. *The Journal of the Acoustical Society of America*, 107(5):2370 – 2378, 2000.

[18] T. Demol, P. Blanquet, and C. Delebarre. Lamb waves generation using a flat multi-element array device. In *Proceedings of the 1995 IEEE Ultrasonics Symposium*, volume 1, pages 791–794, 1995.

[19] R. S. C. Monkhouse, P. D. Wilcox, and P. Cawley. Flexible interdigital PVDF transducers for the generation of Lamb waves in structures. *Ultrasonics*, 35(7):489–498, 1997.

[20] J. L. Rose, S. P. Pelts, and M. J. Quarry. A comb transducer model for guided wave NDE. *Ultrasonics*, 36(1-5):163–169, 1998.

[21] P. D. Wilcox. Omni-directional guided wave transducer arrays for the rapid inspection of large areas of plate structures. *IEEE Transactions on Ultrasonics, Ferroelectrics and Frequency Control*, 50(6):699 – 709, 2003.

[22] P. D. Wilcox, M. Lowe, and P. Cawley. Omnidirectional guided wave inspection of large metallic plate structures using an EMAT array. *IEEE Transactions on Ultrasonics, Ferroelectrics and Frequency Control*, 52(4):653–665, 2005.

[23] V. Giurgiutiu. Tuned lamb wave excitation and detection with piezoelectric wafer active sensors for structural health monitoring. *Journal of Intelligent Material Systems and Structures*, 16(2):291 – 305, 2005.

[24] D. N. Alleyne and P. Cawley. A two-dimensional fourier transform method for the measurement of propagating multimode signals. *The Journal of the Acoustical Society of America*, 89(3):1159 – 1168, 1991.

[25] M. Niethammer, L. J. Jacobs, J. Qu, and J. Jarzynski. Time-frequency representations of Lamb waves. *The Journal of the Acoustical Society of America*, 109(5):1841–1847, 2001.

[26] D. N. Alleyne and P. Cawley. The interaction of Lamb waves with defects. *IEEE Transactions on Ultrasonics, Ferroelectrics and Frequency Control*, 39(3):381–397, 1992.

[27] Y. Cho and J. L. Rose. A boundary element solution for a mode conversion study on the edge reflection of Lamb waves. *The Journal of the Acoustical Society of America*, 99(4):2097–2109, 1996.

[28] M. J. S. Lowe and O. Diligent. Low-frequency reflection characteristics of the S0 Lamb wave from a rectangular notch in a plate. *The Journal of the Acoustical Society of America*, 111(1):64–74, 2002.

[29] M. J. S. Lowe, P. Cawley, J. Y. Kao, and O. Diligent. The low frequency reflection characteristics of the fundamental antisymmetric Lamb wave a_0 from a rectangular notch in a plate. *The Journal of the Acoustical Society of America*, 112(6):2612–2622, 2002.

[30] Cho Y. and Rose J. L. An elastodynamic hybrid boundary element study for elastic guided wave interactions with a surface breaking defect. *International Journal of Solids and Structures*, 37(30):4103 – 4124, 2000.

[31] P. D. Wilcox. A rapid signal processing technique to remove the effect of dispersion from guided wave signals. *IEEE Transaction on Ultrasonics, Ferroelectrics and Frequency Control*, 50(4):419–427, 2003.

[32] D. H. Johnson and D. E. Dudgeon. *Array signal processing: concepts and techniques*. Simon & Schuster, 1992.

[33] H. L. Van Trees. *Optimum Array Processing (Detection, Estimation, and Modulation Theory, Part IV)*. Wiley-Interscience, New York, 1 edition, 2002.

[34] J. Capon. High-resolution frequency-wavenumber spectrum analysis. *Proceedings of the IEEE*, 57(8):1408 – 1418, 1969.

[35] P. Stoica and R. L. Moses. *Introduction to spectral analysis*. Prentice Hall Upper Saddle River, New Jersey, 1997.

[36] B. Widrow, K. Duvall, R. Gooch, and W. Newman. Signal cancellation phenomena in adaptive antennas: Causes and cures. *IEEE Transactions on Antennas and Propagation*, 30(3):469–478, 1982.

[37] H. Hung and M. Kaveh. Focussing matrices for coherent signal-subspace processing. *IEEE Transactions on Acoustics, Speech, and Signal Processing*, 36(8):1272 – 1281, 1988.

[38] T. J. Shan, M. Wax, and T. Kailath. On spatial smoothing for directon-of-arrival estimation of coherent signals. *IEEE Transactions on Acoustics, Speech, and Signal Processing*, 33(4):806 – 811, 1985.

[39] K. W. Lo. Adaptive array processing for wide-band active sonars. *IEEE Journal of Oceanic Engineering*, 29(3):837–846, 2004.

[40] M. Sasso and C. Cohen-Bacrie. Medical ultrasound imaging using the fully adaptive beamformer. In *IEEE International Conference on Acoustics, Speech and Signal Processing, 2005.*, volume 2, pages 489–492, 2005.

[41] J. F. Synnevåg, A. Austeng, and S. Holm. Adaptive beamforming applied to medical ultrasound imaging. *IEEE Transactions on Ultrasonics, Ferroelectrics and Frequency Control*, 54(8):1606–1613, 2007.

[42] Z. Wang, J. Li, and R. Wu. Time-delay and time-reversal-based robust Capon beamformers for ultrasound imaging. *IEEE Transactions on Medical Imaging*, 24(10):1308–1322, 2005.

[43] J. Li, P. Stoica, and Z. Wang. On robust capon beamforming and diagonal loading. *IEEE Transactions on Signal Processing*, 51(7):1702 – 1715, 2003.

[44] J. Li, L. Du, and P. Stoica. Fully automatic computation of diagonal loading levels for robust adaptive beamforming. In *IEEE International Conference on Acoustics, Speech, and Signal Processing,2008*, pages 2325–2328, 2008.

[45] L. Du, J. Li, and P. Stoica. User parameter free approaches to multistatic adaptive ultrasound imaging. In *2008 IEEE International Symposium on Biomedical Imaging: From Macro to Nano (ISBI '08)*, pages 1287 – 1290, 2008.

[46] J. Krolik and D. Swingler. Multiple broad-band source location using steered covariance matrices. *IEEE Transactions on Acoustics, Speech and Signal Processing*, 37(10):1481 – 1494, 1989.

[47] R. Schmidt. Multiple emitter location and signal parameter estimation. In *Proceedings of the RADC Spectrum Estimation Workshop*, pages 243–248, 1979.

[48] G. S. Wagner and T. J. Owens. Broadband eigen-analysis for three-component seismic array data. *IEEE Transactions on Signal Processing*, 43(7):1738 – 1741, 1995.

[49] W. A. K. Deutsch, A. Cheng, and J. D. Achenbach. Self-focusing of Rayleigh waves and Lamb waves with a linear phased array. *Research in Nondestructive Evaluation*, 9(2):81–95, 1997.

[50] P. D. Wilcox, M. J. S. Lowe, and P. Cawley. Lamb and SH wave transducer arrays for the inspection of large areas of thick plates. In *Annual Review of Progress in QNDE*, volume 19A, pages 1049 – 1056, 2000.

[51] P. D. Wilcox. Omni-directional guided wave transducer arrays for the rapid inspection of large areas of plate structures. *IEEE Transactions on Ultrasonics, Ferroelectrics and Frequency Control*, 50(6):699 – 709, 2003.

[52] P. Fromme, P. D. Wilcox, M. J. S. Lowe, and P. Cawley. On the development and testing of a guided ultrasonic wave array for structural integrity monitoring. *IEEE Transactions on Ultrasonics, Ferroelectrics and Frequency Control*, 53(4):777 – 785, 2006.

[53] V. Giurgiutiu and J. Bao. Embedded Ultrasonic Structural Radar for the Nondestructive Evaluation of Thin-Wall Structures. In *Proceedings of the 2002 ASME International Mechanical Engineering Congress*, pages 17–22, 2002.

[54] L. Yu and V. Giurgiutiu. Design, implementation, and comparison of guided wave phased arrays using embedded piezoelectric wafer active sensors for structural health monitoring. In *Proceedings of SPIE*, volume 6173, pages 61731M1–61731M12, 2006.

[55] E. Moulin, N. Bourasseau, J. Assaad, and C. Delebarre. Lamb wave beam-steering for integrated health monitoring applications. In *Proceedings of SPIE*, volume 5046, pages 124–131, 2003.

[56] S. Sundararaman, D. E. Adams, and E. J. Rigas. Structural damage identification in homogeneous and heterogeneous structures using beamforming. *Structural Health Monitoring*, 4(2):171–190, 2005.

[57] J. Rajagopalan, K. Balasubramaniam, and C. V. Krishnamurthy. A phase reconstruction algorithm for Lamb wave based structural health monitoring of anisotropic multilayered composite plates. *The Journal of the Acoustical Society of America*, 119(2):872–878, 2006.

[58] F. Yan and J. L. Rose. Guided wave phased array beam steering in composite plates. In *Proceedings of SPIE*, volume 6532, pages 65320G.1–65320G.9, 2007.

[59] A. Velichko and P. D. Wilcox. Guided wave arrays for high resolution inspection. *The Journal of the Acoustical Society of America*, 123(1):186 – 196, 2008.

[60] F. Yan, R. L. Royer jr, and J. L. Rose. Ultrasonic Guided Wave Imaging Techniques in Structural Health Monitoring. *Journal of Intelligent Material Systems and Structures*, 21(3):377–384, 2010.

[61] M. Fink, C. Prada, F. Wu, and D. Cassereau. Self focusing in inhomogeneous media with time reversal acousticmirrors. In *Proceedings of the IEEE Ultrasonics Symposium*, pages 681–686, 1989.

[62] D. N. Alleyne, T. P. Pialucha, and P. Cawley. A signal regeneration technique for long-range propagation of dispersive lamb waves. *Ultrasonics*, 31(3):201 – 204, 1993.

[63] R. K. Ing and M. Fink. Time recompression of dispersive lamb waves using a time reversal mirror-application to flaw detection in thin plates. In *Proceedings of the IEEE Ultrasonics Symposium*, volume 1, pages 659–664, 1996.

[64] R. K. Ing and M. Fink. Self-focusing and time recompression of Lamb waves using a time reversal mirror. *Ultrasonics*, 36(1):179–186, 1998.

[65] D. P. Jansen and D. A. Hutchins. Immersion tomography using Rayleigh and Lamb waves. *Ultrasonics*, 30(4):245–254, 1992.

[66] W. Wright, D. Hutchins, D. Jansen, and D. Schindel. Air-coupled Lamb wave tomography. *IEEE Transactions on Ultrasonics, Ferroelectrics, and Frequency Control*, 44(1):53–59, 1997.

[67] J. C. P. McKeon and M. K. Hinders. Parallel projection and crosshole Lamb wave contact scanning tomography. *The Journal of the Acoustical Society of America*, 106(5):2568–2577, 1999.

[68] C. H. Wang, J. T. Rose, and F. K. Chang. A synthetic time-reversal imaging method for structural health monitoring. *Smart Materials and Structures*, 13(2):415–423, 2004.

[69] G. Konstantinidis, B. W. Drinkwater, and P. D. Wilcox. The temperature stability of guided wave structural health monitoring systems. *Smart Materials and Structures*, 15(4):967–976, 2006.

[70] J. E. Michaels and T. E. Michaels. An integrated strategy for detection and imaging of damage using a spatially distributed array of piezoelectric sensors. In *Proc. of SPIE*, volume 6532, pages 653203.1–653203.12, 2007.

[71] P. D. Wilcox, A. J. Croxford, J. E. Michaels, Y. Lu, and B. W. Drinkwater. A Comparison of Temperature Compensation Methods for Guided Wave Structural Health Monitoring. In *Review of Progress in Quantitative Nondestructive Evaluation*, volume 975, pages 1453–1460, 2008.

[72] J. E. Michaels, J. S. Hall, and T. E. Michaels. Adaptive imaging of damage from changes in guided wave signals recorded from spatially distributed arrays. In *Proceedings of SPIE*, volume 7295, pages 729515–729515–11, 2009.

[73] R. Sicard, J. Goyette, and D. Zellouf. A SAFT algorithm for Lamb wave imaging of isotropic plate-like structures. *Ultrasonics*, 39(7):487–494, 2002.

[74] R. Sicard, A. Chahbaz, and J. Goyette. Guided Lamb waves and L-SAFT processing technique for enhanced detection and imaging of corrosion defects in plates with small depth-to wavelength ratio. *IEEE Transactions on Ultrasonics, Ferroelectrics and Frequency Control*, 51(10):1287–1297, 2004.

[75] H. Krim and M. Viberg. Two decades of array signal processing research: the parametric approach. *IEEE Signal processing magazine*, 13(4):67–94, 1996.

[76] T. Cicero, P. Cawley, F. Simonetti, and S.I. Rokhlin. Potential and Limitations of a Deconvolution Approach for Guided Wave Structural Health Monitoring. *Structural Health Monitoring*, 8(5):381, 2009.

[77] P. Cawley. The impedance method of non-destructive inspection. *NDT international*, 17(2):59–65, 1984.

[78] P. Cawley. The sensitivity of the mechanical impedance method of nondestructive testing. *NDT international*, 20(4):209–215, 1987.

[79] R. D. Adams and P. Cawley. A review of defect types and nondestructive testing techniques for composites and bonded joints. *NDT International*, 21(4):208–222, 1988.

[80] A. Migliori and J. L. Sarrao. *Resonant ultrasound spectroscopy: applications to physics, materials measurements, and nondestructive evaluation*. Wiley-Interscience, 1997.

[81] J. Ling, T. Yardibi, X. Su, H. He, and J. Li. Enhanced channel estimation and symbol detection for high speed multi-input multi-output underwater acoustic communications. *The Journal of the Acoustical Society of America*, 125(5):3067–3078, 2009.

[82] P. Stoica, J. Li, and J. Ling. Missing Data Recovery Via a Nonparametric Iterative Adaptive Approach. *IEEE Signal Processing Letters*, 16(4):241–244, 2009.

[83] T. Yardibi, Jian Li, P. Stoica, Xue M., and A. B. Baggeroer. Source localization and sensing: A nonparametric iterative adaptive approach based on weighted least squares. *IEEE Transactions onAerospace and Electronic Systems*, 46(1):425–443, 2010.

[84] E. Gudmundson, P. Stoica, J. Li, A. Jakobsson, M. D. Rowe, J. A. S. Smith, and J. Ling. Spectral estimation of irregularly sampled exponentially decaying signals with applications to rf spectroscopy. *Journal of Magnetic Resonance*, 203(1):167 – 176, 2010.

Acta Universitatis Upsaliensis

Digital Comprehensive Summaries of Uppsala Dissertations from the Faculty of Science and Technology 732

Editor: The Dean of the Faculty of Science and Technology

A doctoral dissertation from the Faculty of Science and Technology, Uppsala University, is usually a summary of a number of papers. A few copies of the complete dissertation are kept at major Swedish research libraries, while the summary alone is distributed internationally through the series Digital Comprehensive Summaries of Uppsala Dissertations from the Faculty of Science and Technology. (Prior to January, 2005, the series was published under the title "Comprehensive Summaries of Uppsala Dissertations from the Faculty of Science and Technology".)

Distribution: publications.uu.se
urn:nbn:se:uu:diva-122189

ACTA
UNIVERSITATIS
UPSALIENSIS
UPPSALA
2010